Acta Biochim Biophys Sin xxxx, xx(xx): xx–xx
https://cstr.cn/32197.14.abbs.2026084
https://doi.org/10.3724/abbs.2026084
Original Article

Original Article

HDAC6 promotes osimertinib resistance evolution in non-small cell lung cancer by activating EGFR degradation through the ubiquitin-proteasome pathway

Cheng Yang[1,†], Danlei Xu[1,2,†], Zifang Zhu[1,5,†], Zhen Kang[1,†], Kangkang Ren[1,2], Yihan Yang[1,2,3], Ye Huang[1,2,3], Wei Zhang[1,2,3], Jun Che[4], Xinping Xu[1,2,3], and Xiaolei Li[1,2,3,*]

[1]Jiangxi Provincial Key Laboratory of Respiratory Diseases, Jiangxi Institute of Respiratory Diseases, Department of Respiratory and Critical Care Medicine, The First Affiliated Hospital, Jiangxi Medical College, Nanchang University, Nanchang 330006, China, [2]China-Japan Friendship Jiangxi Hospital, National Regional Center for Respiratory Medicine, Nanchang 330200, China, [3]Jiangxi Clinical Research Center for Respiratory Diseases, Nanchang 330006, China, [4]Department of Biochemistry, School of Medicine, Southern University of Science and Technology, Shenzhen 518055, China, and [5]Jiangxi Institute of Technology, Nanchang 330098, China
[†]These authors contributed equally to this work.
*Correspondence address. E-mail: xiaoleili1225@163.com/ndyfy05473@ncu.edu.cn

Received 23 September 2025 Accepted 21 April 2026 Published 23 June 2026

Abstract

Osimertinib is the standard first-line treatment for patients with non-small cell lung cancer (NSCLC) harboring *EGFR*-sensitive mutations. However, drug resistance inevitably develops, highlighting the critical need for strategies to overcome this resistance and prolong therapeutic efficacy. Understanding the mechanisms underlying drug resistance is essential, and drug-resistant cell models serve as valuable tools for investigating acquired resistance. In this study, we establish an osimertinib resistance evolution model *in vitro* by continuous high-dose drug induction and identify cell lines exhibiting "permanent" resistance to osimertinib (osimertinib resistant, OR). Transcriptome sequencing (RNA-seq), gain- and loss-of-function assay, including lentiviral-mediated overexpression and RNAi knockdown, pharmacological inhibition, and protein degradation analysis reveal significant alterations in genes associated with epigenetic regulation, notably a marked upregulation of histone deacetylase 6 (HDAC6) in OR cells. Knockdown of *HDAC6* or pharmacological inhibition of HDAC6 restores the sensitivity of OR cells to osimertinib, whereas overexpression of HDAC6 in sensitive cells reduces drug efficacy and accelerates the onset of resistance. Furthermore, we find that HDAC6 upregulation promotes EGFR degradation, thereby contributing to resistance. Collectively, our findings demonstrate the utility of drug resistance evolution models in identifying key resistance factors. HDAC6 plays a pivotal role in osimertinib resistance, and targeting HDAC6 may represent a novel therapeutic strategy to overcome resistance and enhance treatment efficacy.

Key words drug resistance, acquired resistance, EGFR inhibition, HDAC6, EGFR degradation

Introduction

In 2022, lung cancer accounted for approximately 2.5 million new cases and 1.8 million deaths worldwide [1], underscoring its persistent global health burden [2]. The identification of driver genes and the development of targeted therapies have substantially improved treatment outcomes for lung cancer patients with specific genetic mutations [3]. However, the inevitable emergence of drug resistance remains a major clinical challenge, adversely affecting patient survival and limiting the durability of treatment response. Therefore, extending the effective use of targeted therapies and delaying or overcoming resistance represent urgent and unresolved priorities in clinical oncology.

EGFR was the first driver gene identified in lung cancer [4]. Osimertinib, a third-generation EGFR tyrosine kinase inhibitor (TKI), is now used as a first-line treatment in clinical practice [5]. It extends progression-free survival (PFS) in lung cancer patients to

© The Author(s) 2026. This is an open access article distributed under the terms of the Creative Commons Attribution License (https://creativecommons.org/licenses/by/4.0/).

10–18.9 months [6,7], with a median overall survival (OS) of 26.8–38.6 months [7]. Several studies have characterized key mechanisms of osimertinib resistance, including target mutations, bypass signaling activation and histological transformation [8,9]. However, these studies have largely focused on patients after resistance has already developed. Drug resistance is a dynamic process, and understanding its evolution along with developing effective interventions is critical to overcoming clinical resistance. Traditional resistance models typically involve gradually increasing drug concentrations to induce resistance, yielding a homogeneous population of resistant cells [10]. In contrast, high-dose "hard-hit" approaches more closely recapitulate the clinical onset of resistance and provide a superior platform for mechanistic investigation [11,12]. In this approach, a high concentration of osimertinib eliminate most sensitive cells, while the surviving cells gradually evolve drug-resistant traits under continuous drug pressure and ultimately establish stable drug resistance through adaptive mutagenesis [13].

Epigenetic modifications involve heritable changes in gene expression that occur without altering the DNA sequence. These modifications include DNA methylation, histone modification, chromatin remodeling, noncoding RNA regulation, nucleosome positioning, and genomic imprinting [14]. By influencing chromatin structure and function, they play a crucial role in determining gene activation or silencing, thereby regulating processes such as cell differentiation, development, and adaptation to environmental cues. Histone deacetylases (HDACs) are key enzymes that modulate the acetylation levels of histones and other proteins. By removing acetyl groups from lysine residues on histone or nonhistone substrates, HDACs promote chromatin condensation and suppress transcription activity [15,16]. Beyond histone targeting, HDACs can also interact with nonhistone proteins, exerting dual oncogenic and tumor-suppressive functions in cancer. They influence various cellular processes, including stemness, proliferation, apoptosis, differentiation, angiogenesis, migration and invasion, thereby contributing to cancer progression [17]. Notably, elevated HDAC expression is often associated with tumorigenesis, with HDAC6 emerging as a particularly significant player due to its involvement in cancer advancement [18–20] and the regulation of drug resistance [21,22]. Accumulating evidence links aberrant HDAC6 activity to multitherapy resistance in cancer, encompassing chemotherapy, targeted agents, and immunotherapy. In lung cancer, HDAC6 overexpression confers platinum resistance by destabilizing phospho-ATR/Chk1 and blocking p53-mediated apoptosis [23]. In glioblastoma, HDAC1/2/6-driven deacetylation of specificity protein 1 (Sp1) expands therapy-resistant cancer stem cell (CSC) populations, fueling temozolomide resistance [24]. Resistance mechanisms in non-small cell lung cancer (NSCLC) further involve USP10-mediated HDAC6 stabilization, which exacerbates cisplatin resistance [25]. HDAC6 promotes sorafenib resistance in NSCLC by stabilizing EGFR and suppressing apoptosis [26]. Mechanistically, it sustains gefitinib resistance through dual regulation of EGFR stability and ERK phosphorylation [27]. Furthermore, HDAC6 induces TGF-β1-mediated epithelial-mesenchymal transition (EMT) via modulation of α-tubulin acetylation, driving TKI resistance [28]. Beyond targeted therapy and chemotherapy, HDAC6 critically regulates immunotherapy outcomes by orchestrating remodeling of the tumor immune microenvironment through dual modulation of immune cell recruitment and functional polarization. Clinically, elevated HDAC6 expression correlates significantly with diminished therapeutic response to immune checkpoint inhibitors (ICIs) in NSCLC patients, establishing HDAC6 as a predictive biomarker of ICI refractoriness [29]. At the mechanistic level, pharmacological HDAC6 inhibition fosters an immunopermissive tumor niche via two synergistic pathways: (1) attenuation of immunosuppressive cytokine networks (particularly IL-6 and IL-1β signaling cascades) and (2) functional impairment of regulatory T cell (Treg)-mediated immune suppression [29]. Complementary murine studies further substantiate that HDAC6 ablation potentiates macrophage-mediated antitumor responses through coordinated upregulation of antigen presentation machinery (MHC class II) and T-cell costimulatory signals (CD86), effectively bridging innate and adaptive immunity [30]. In summary, dysregulated HDAC6 expression drives tumor resistance, and pharmacological targeting of HDAC6 represents a promising strategy to circumvent acquired drug resistance.

In this study, we established a cellular model to investigate acquired resistance mechanisms and identified drug-resistant cell lines driven by EGFR loss. Characterization of these resistant clones revealed elevated HDAC6 expression in conjunction with reduced EGFR levels. Further mechanistic studies demonstrated that HDAC6 modulates EGFR protein stability through the ubiquitin-proteasome pathway, thereby influencing sensitivity to osimertinib. Notably, pharmacological inhibition of HDAC6 delayed the onset of acquired resistance to osimertinib. Collectively, our findings suggest a novel therapeutic strategy to overcome resistance mediated by EGFR loss.

Methods and Materials

Chemical reagents and antibodies

Osimertinib (S7297; Selleck, Houston, USA; HY-15772; MCE, Monmouth Junction, USA), tubastatin A (TAA; HY-13271A; MCE, Monmouth Junction, USA), and gefitinib (HY-50895; MCE) were commercially obtained. Osimertinib from Selleck was exclusively applied to Figure 1 experiments, and all remaining tests employed osimertinib from MCE. Replication of Figure 1 assays with osimertinib from MCE confirmed comparable cellular drug sensitivity for both reagents. Antibodies were sourced from Cell Signaling Technology (Beverly, USA) or Proteintech (Chicago, USA); detailed information is provided in Supplementary Table S1.

Cell culture and cell line generation

Non-small cell lung cancer cell line PC-9 (delE746_A750) was obtained from EK-Bioscience (CC-Y1418; Shanghai, China). PC-9 cell line was cultured in RPMI-1640 medium (C11875500BT; Gibco, Grand Island, USA) supplemented with 10% fetal bovine serum (FBS; FSP500; ExCell Bio, Suzhou, China) and antibiotics (100 U/mL penicillin and 100 μg/mL streptomycin) (Transgen, Beijing, China). Cells were cultured at 37°C in a 5% CO_2 incubator (BB150; Thermo Fisher Scientific, Waltham, USA) and subcultured with Typsin-EDTA (FG301-1; Transgen) before they reached confluence.

To generate PC-9 naïve single-cell clones, PC-9 cells were plated in 96-well plates at a density of one cell per well and cultured for two weeks to allow the formation of single-cell colonies. A minimum of 10 single-cell clones were isolated and expanded. Four of these clones were randomly selected for testing their sensitivity to EGFR-TKIs, especially osimertinib and gefitinib. Clones exhibiting sensitivity to both osimertinib and gefitinib were designated naïve PC-9 cells (nPC-9 cells), while clones resistant to

gefitinib were classified as primary gefitinib-resistant PC-9 cells (PC-9 GR cells). The cellular morphology of PC-9 naïve single-cell and parental cells were observed and photographed using an EVOS 5000 microscope (Thermo Fisher Scientific).

To generate osimertinib-resistant (OR) cell lines, nPC-9 cells were seeded into 100-mm dishes and were allowed to reach 80%–90% confluence. Osimertinib was then added to the medium to a final concentration of 80 nM (the lowest concentration that induces substantial cell death). Media (containing 80 nM osimertinib) was exchanged every 3–4 days for approximately one month. Individual colonies were isolated and expanded for characterization. Three independent clone cell lines were randomly chosen, and their sensitivity to osimertinib was assessed. OR cell lines were established. The morphology of OR cells was observed and imaged using the EVOS 5000 microscope.

Cell survival assay

Cell proliferation and survival assays were conducted using either the MuviCyte™ Live Cell Imaging System (PerkinElmer, Waltham, USA) or the Cell Counting Kit-8 assay (CCK-8; GK10001; GLPBIO, Montclair, USA). Briefly, exponentially growing cells were seeded into 96-well plates and treated with varying concentrations of the drug, according to the specific experimental objectives. Cellular images were captured using the MuviCyte™ Live Cell Imaging System, and cell survival was quantified based on the cell area. For CCK-8 assay, cell viability was determined by measuring the absorbance at 450 nm, and the cell survival fraction was calculated accordingly. To assess the interaction between osimertinib and TAA, Synergy Finder (version 3.0) was utilized to calculate the synergy score of the two drugs based on the Bliss model. Ten different concentrations of each drug were tested to create a total of 100 unique drug combinations. After 72 h of exposure of drugs, osimertinib and TAA, cell viability was assessed using the CCK-8 assay. The synergy score for the two drugs was calculated using the Synergy Finder tool. The interpretation of the synergy score is as follows: a score of less than −10 indicates a likely antagonistic interaction between the two drugs; a score between −10 and 10 suggests an additive interaction; and a score larger than 10 implies a synergistic interaction between the two drugs.

Proliferation and survival assays in lung cancer organoids

The lung cancer organoid model was derived from a treatment-naïve lung adenocarcinoma patient using tumor tissue acquired by lung puncture and possesses both EGFR amplification and the E746_A750del mutation. Detailed information can be found in Supplementary Table S2.

Lung cancer organoids were suspended in Organoid Culture Extracellular Matrix (ECM; M315066; bioGenous, Shanghai, China) and seeded into 24-well plates (20 μL/well). Cultures were maintained in RPMI 1640 supplemented with 10% FBS at 37°C under 5% CO_2. Following approximately 7 days of growth in ECM, organoids were treated with osimertinib for 4 days. Organoid viability was assessed using a luminescence-based 3D ATP Detection kit (CP-00850; Origen Biotech, Guangzhou, China) according to the manufacturer's protocol. Briefly, an equal volume of room temperature-equilibrated 3D ATP detection reagent was added to the culture medium. The plates were agitated for 5 min to ensure homogeneous organoid distribution prior to luminescence measurement. For comparative analysis, PC-9 cells were cultured under organoid-like conditions. Briefly, cells (in 20 μL ECM) were seeded in a 24-well plate at 3000 cells/well and subjected to osimertinib treatment. Viability was quantified using the same 3D ATP detection assay as described for lung cancer organoids. Lung cancer organoids were treated with osimertinib, TAA, or combination therapy. Dynamic morphological changes of organoids were captured on days 0, 3, 5, and 7 using the EVOS 5000 microscope.

Colony formation assay

Cells were seeded onto 100-mm tissue culture dishes or 6-well plates depending on the aims of the experiments and incubated for 24 h to allow attachment. Cells were treated with drugs according to the experimental requirements, and the medium was changed every three days. Then, the cells were cultured for 14 days to form colonies. The colonies were fixed with 6% glutaraldehyde (v/v) and stained with 0.5% (w/v) crystal violet (C8470; Solarbio, Beijing, China). Colonies containing > 50 cells were counted, and the *HPRT* gene mutation frequency was calculated, considering the plating efficiency of the control dish. At least three independent experiments were performed. Each experiment used duplicate dishes.

RNA-Seq and differentially expressed gene analysis

Total RNA was extracted using TRIzol reagent (ET111-01; Transgen) following the manufacturer's protocol. RNA purity and concentration were measured using a NanoDrop 2000 spectrophotometer (Thermo Fisher Scientific), while RNA integrity was assessed by an Agilent 2100 Bioanalyzer (Agilent Technologies, Santa Clara, USA). The transcriptome library was constructed using the VAHTS University V5 RNA-seq Library Prep Kit (Vazyme Biotech, Nanjing, China) according to the manufacturer's instructions. RNA sequencing and subsequent analysis were performed by OE Biotech (Shanghai, China).

The libraries were sequenced on an Illumina NovaSeq 6000 platform (Illumina, San Diego, USA), and 150 bp paired-end reads were generated. Approximately 50 M raw reads for each sample were generated. Raw reads in fastq format were first processed using fastp1, and the low-quality reads were removed to obtain the clean reads. Then, approximately 50 M clean reads for each sample were retained for subsequent analyses. The clean reads were mapped to the reference genome using HISAT22. The FPKM3 of each gene was calculated, and the read counts of each gene were obtained by HTSeq-count4. PCA was performed using R (v3.2.0) to evaluate the biological duplication of samples. Genes associated with epigenetic regulation are highlighted in the volcano plot. Uses $|\log2FC| = 0.5849$ (FC = 1.5) and P value = 0.05 as the cutoff criteria. Genes with log2FC > 0.5849 and P value < 0.05 were defined as upregulated, while those with log2FC < −0.5849 and P value < 0.05 were defined as downregulated. Red dots represent significantly upregulated genes, while blue dots indicate significantly downregulated genes.

Cell competition assay

Stable PC-9 cell lines expressing HDAC6 with GFP labeling were generated, while parental PC-9 cells served as GFP-negative controls. The two cell populations were cocultured at a 1:1 ratio in 6-well plates. Following cell adhesion, cultures were treated with either 80 nM osimertinib or vehicle control, as indicated by the experimental conditions. The treatment medium was refreshed every 3–4 days to maintain consistent drug exposure. Cells were

harvested at designated time points (days 0, 1, 2 and 3 post treatment). The relative proportions of GFP-positive and GFP-negative populations were analyzed using a CytoFLEX S flow cytometer (Beckman Coulter, Brea, USA).

Western blot analysis

Cell extracts were prepared on ice with RIPA lysis buffer (C1053; Applygen Technologies, Beijing, China) supplemented with protease inhibitors (GK10014; GLPBIO), phosphatase inhibitors (GK10011; GLPBIO) and 1 mM PMSF (P0100; Solarbio), followed by pulse sonication for 10 s. The cell extracts were boiled for 5 min at 95°C, and the same amount of protein was resolved via 10% SDS-PAGE and transferred onto PVDF membranes (HybondTM P 0.45 PVDF 10600023; Amersham, Chicago, USA). After being blocked with 5% nonfat milk or 5% BSA (depending on the primary antibody used) in 1× TBST (Tris-buffered saline containing 0.05% Tween 20) at room temperature for 1 h, the membrane was incubated with the primary antibodies (Supplementary Table S1) overnight at 4°C, followed by incubation with peroxidase-conjugated secondary antibodies AffiniPure goat anti-mouse IgG(H+L) (150976) or goat anti-rabbit IgG(H+L) (151083; Jackson ImmunoResearch Laboratories, West Grove, USA). Western blot analysis was performed with an enhanced chemiluminescence system (ChemiDocTM Imaging System; Bio-Rad, Hercules, USA).

Quantitative real-time PCR (qRT-PCR)

The total RNAs were extracted using TRIzol extraction reagent and was reversely transcribed to cDNAs. Then, the cDNAs were mix with PerfectStart® Green qPCR SuperMix (+Universal Passive Reference Dye) (AQ602-01; Transgen) and primers for q-PCR assay carried out on real-time PCR system (Quant Studio DX; Thermo Fisher Scientific). The primer sequences used in this study were as follows: *GAPDH* forward, 5′-CAAATTCCATGGCACCGTCAA-3′ and reverse, 5′-AGCATCGCCCCACTTGATTT-3′; *EGFR* forward, 5′-AGC AGAGACCCACACTACCA-3′ and reverse, 5′-GTAGTCAGGGTTGTC CAGGC-3′; and *HDAC6* forward, 5′-CTGGCGGAGTGGAAGAACC-3′ and reverse, 5′-TCTGCCTACTTCTTCGCTGC-3′. The expression of each gene was normalized to the corresponding *GAPDH* threshold cycle (Ct) values by the $2^{-\Delta\Delta Ct}$ method.

siRNA-mediated *HDAC6* knockdown and functional assays

HDAC6-specific siRNA duplexes (Locus ID 10013, SR322962; Origene Biotech) were used for gene silencing. The sequences were of siRNAs were: siHDAC6#1: 5′-GCAUCAAGCUCAACUGAAA-3′; siHDAC6#2: 5′-GCAGAUGAGCUGCAAGAAA-3′; and Scramble siRNA, 5′-GAGCCCGTGGTATTGGTAGTTT-3′. PC-9 OR cells were seeded in 6-well plates and transfected with 50 nM siRNA using the siTran 2.0 transfection reagent (TT320001; Origene Biotech) upon reaching adequate adherence. After 48 h of transfection, cells were harvested for subsequent experiments. The *HDAC6*-silencing efficiency was confirmed by qRT-PCR and western blot analysis. Transfected cells were seeded in 96-well plates at 3000 cells/well and monitored continuously using the MuviCyte™ Live Cell Imaging System to compare proliferation among the following groups: siScramble (negative control), siHDAC6#1, and siHDAC6#2. For clonogenic survival analysis, transfected cells were plated at 200 cells/well in 6-well plates. After adherence, cells were treated with increasing concentrations of osimertinib (0, 500, 1000, and 2000 nM). Fresh medium was replenished every 3 days. After ~14 days, colonies were fixed with methanol, stained with crystal violet, imaged, and quantified using ImageJ.

Establishment of a stable HDAC6-overexpressing cell line

We purchased the HDAC6 expression plasmid (pLV3-CMV-HDAC6 (human)-3×FLAG-CopGFP-Puro; P56497) and the empty vector control (pLV3-CMV-MCS-3×FLAG-CopGFP-Puro; P40122) from MIAOLING BIO (Wuhan, China). These plasmids, along with the packaging plasmids psPAX2 and pMD2.G (12260 and 12259; Addgene, Watertown, USA), were cotransfected into 293T cells using PEI transfection reagent (HY-K2014; MCE). The viral supernatant was harvested and used to infect PC-9 cells. PC-9 HDAC6 OE, the stable HDAC6-expressing single-cell clone, was then selected with puromycin (1 μg/mL).

Cell apoptosis analysis

PC-9 cells were treated with osimertinib (80 nM), TAA (10 μM), or the combination of both drugs for 72 h. Following treatment, cells were harvested by trypsinization, washed twice with cold PBS and stained using an Annexin V-FITC/PI apoptosis detection kit (40302ES60; Yeasen Biotechnology, Shanghai, China) according to the manufacturer's instructions. Cells were then analyzed using a CytoFLEX S flow cytometer (Beckman Coulter). Apoptotic populations were defined as follows: early apoptotic (Annexin V-FITC$^+$ PI$^-$), late apoptotic (Annexin V-FITC$^+$PI$^+$), and necrotic (Annexin V-FITC$^-$PI$^+$) cells. Data analysis was performed using FlowJo (10.6.2) within a minimum of 10,000 events collected per sample.

Co-immunoprecipitation analysis

For co-immunoprecipitation (Co-IP) analysis, PC-9 OR cells were pretreated with the proteasome inhibitor MG132 (10 μM) for 6 h to stabilize protein interactions. Cells were then lysed in 400 μL ice-cold IP lysis buffer (G2038; Servicebio, Wuhan, China) supplemented with protease and phosphatase inhibitors, followed by incubation on ice for 15 min. Lysates were clarified by centrifugation at 14,000 *g* for 20 min at 4°C. For preclearing, 30 μL of Protein G-agarose beads (11243233001; Merck, San Diego, USA) were equilibrated with 500 μL of IP buffer and washed twice. Clarified lysates were incubated with the prewashed beads for 1 h at 4°C with end-over-end rotation. The precleared supernatant was then immunoprecipitated for 1 h at 4°C with either anti-EGFR antibody (4267T; 1:400; Cell Signaling Technology) or rabbit IgG isotype control (30000-0-AP; 1:400; Proteintech). Immune complexes were captured by adding 30 μL of Protein G-agarose beads and incubating for 1 h at 4°C. Beads were washed 4 times with 500 μL of ice-cold IP buffer, with complete aspiration between washes. Bound proteins were eluted by boiling in 30 μL of 2× loading buffer (95°C, 5 min) and analyzed by SDS-PAGE followed by immunoblotting.

Xenograft tumor model and therapeutic intervention

Female BALB/nude mice (4–6 weeks) were purchased from GemPharmatech (Nanjing, China). All animals were maintained under specific pathogen-free (SPF) conditions with a regular 12-h light/dark cycle. To generate subcutaneous xenografts, OR cells and parental nPC-9 cells suspended in a mixture 1:1 (v/v) of media without serum and Matrigel (1×10^7 cells in 100 μL) were inoculated

into the flanks of the mice. When tumor volumes reached approximately 90 mm^3, the PC-9 tumor-bearing mice were randomly divided into four experimental groups: (1) vehicle control, (2) osimertinib monotherapy (10 mg/kg), (3) TAA monotherapy (50 mg/kg), and (4) combination therapy with osimertinib and TAA. OR tumor-bearing mice were divided into two groups (vehicle control and osimertinib monotherapy). Drugs were administered orally by gavage. Tumor dimensions (length and width) and mouse body weights were measured every two days. Tumor volume was calculated using the formula: Volume = (Length × $Width^2$)/2. At the end of experiment, all mice were euthanized by cervical dislocation. Tumors were excised, photographed, and weighed for subsequent analysis. All animal procedures were reviewed and approved by the Institutional Animal Care and Use Committee of the First Affiliated Hospital of Nanchang University (approval number: SYXK(Gan)2024-0006) and were conducted in strict compliance with the National Institutes of Health Guide for the Care and Use of Laboratory Animals.

Statistical analysis

Data from two or three independent experiments are expressed as the mean ± standard deviation (SD). Statistical analysis was performed using GraphPad Prism 5. Two-group comparisons were conducted with unpaired two-tailed Student's *t*-test, and F-test was used to test homogeneity of variance before t analysis. while multigroup comparisons were assessed by one-way ANOVA. $P < 0.05$ was considered statistically significant.

Results

Establishment of naïve single-cell clones and acquisition of osimertinib resistance

In this study, we established a panel of single-cell clones derived from the PC-9 cell line as a model for investigating acquired drug resistance (Figure 1A). Four individual clones were randomly selected, and their sensitivity to osimertinib and gefitinib was compared to that of the parental PC-9 cells. Our data demonstrated that three of the clones (nPC-9#1, #2 and #3) exhibited enhanced sensitivity to both osimertinib and gefitinib compared to the parental PC-9 cell line (Figure 1A). In contrast, one clone (nPC-9#9) was resistant to gefitinib but sensitive to osimertinib (Figure 1A). Additionally, we examined the cell morphology of the naïve PC-9 clones in comparison to the parental PC-9 cells and found no significant morphological differences between them (Figure 1B and Supplementary Figure S1). These findings suggest that naïve PC-9 clones are suitable for use in studies aimed at understanding the evolution of drug resistance.

To generate OR cells, we used osimertinib at a lethal concentration to treat nPC-9#3 cells. During the osimertinib treatment procedure (Figure 1C and Supplementary Figure S2), small colonies were observed among the overall cell population (Supplementary Figure S3). As treatment continued, the majority of the cells died, while some cell clones began to expand. By day 13, most of the cells had died, and the surviving clones became more distinguishable (Supplementary Figure S3). These surviving colonies were isolated and expanded. Three individual colonies were randomly selected for further analysis. Morphologically, these resistant clones exhibited distinct differences compared to the parental PC-9 cells (Figure 1D). While PC-9 cells are characterized by a typical epithelial-like morphology, the OR cells demonstrated more defined intercellular boundaries, a tendency to grow in cluster formations, and a "cobblestone" appearance. Furthermore, sensitivity assays revealed that these OR clones were significantly resistant to osimertinib treatment (Figure 1E,F). Collectively, these data confirm the successful establishment of acquired osimertinib resistance models and the generation of distinct OR clones. Meanwhile, since the process of obtaining OR clones via this method coincides with the development of osimertinib resistance, we consequently established an *in vitro* cellular model to simulate the evolutionary progression of osimertinib resistance (Figure 1C and Supplementary Figure S3).

HDAC6 is upregulated in OR cells at the transcriptional and protein levels

To analyze gene expression changes associated with osimertinib resistance, RNA sequencing was performed on parental nPC-9 cells and OR cells. Significant differential gene expression was observed between OR and parental cells, with notable alterations in deacetylase family genes in OR/gefitinib-resistant (GR) cells (Figure 2A and Supplementary Figure S4). Specifically, HDAC4 and HDAC6 were upregulated, while HDAC1 was significantly downregulated (Figure 2B). Protein level validation confirmed that HDAC6 was consistently elevated across multiple OR/GR cell clones (Figure 2C). In contrast, HDAC1 and HDAC4 levels increased in OR clones but decreased in GR clones (Figure 2C,D). Collectively, these results demonstrate that HDAC6 is significantly upregulated in OR cells at both the transcriptional and protein levels. We further examined HDAC6 expression in lung adenocarcinoma (LUAD) using The Cancer Genomes Atlas (TCGA) data through the UALCAN platform. *HDAC6* mRNA was significantly upregulated in LUAD tissues compared with adjacent normal tissues ($P = 1.402 \times 10^{-6}$; Supplementary Figure S5). These findings suggest that HDAC6 overexpression may contribute to LUAD pathogenesis but does not independently influence overall patient survival.

Knockdown of *HDAC6* by RNAi improves osimertinib sensitivity of PC-9 OR cells

To determine whether elevated HDAC6 expression contributes to drug resistance in OR cells, we utilized siRNA to knock down *HDAC6* and validated the efficiency of the knockdown through western blot analysis and RT-PCR (Figure 3A–C). Our results showed that *HDAC6* knockdown significantly reduced the proliferation rate of OR cells, with the siHDAC6 group growing slower than the control group (Figure 3D,E). Furthermore, we assessed the impact of *HDAC6* knockdown on OR cell sensitivity to osimertinib. The data revealed that knocking down *HDAC6* increased the sensitivity of OR cells to osimertinib (Figure 3E,F). Next, we evaluated the effect of *HDAC6* knockdown on EGFR expression and found that reduced HDAC6 levels upregulated EGFR expression (Figure 3A,C and Supplementary Figure S6A). A similar effect was observed in PC-9 WT cells (Supplementary Figure S6B,C). In summary, elevated HDAC6 expression is associated with drug resistance in OR cells, and targeting HDAC6 enhances their sensitivity to treatment.

The HDAC6 inhibitor TAA improves osimertinib sensitivity in PC-9 OR cells

We found that siRNA-mediated knockdown of *HDAC6* in OR cells

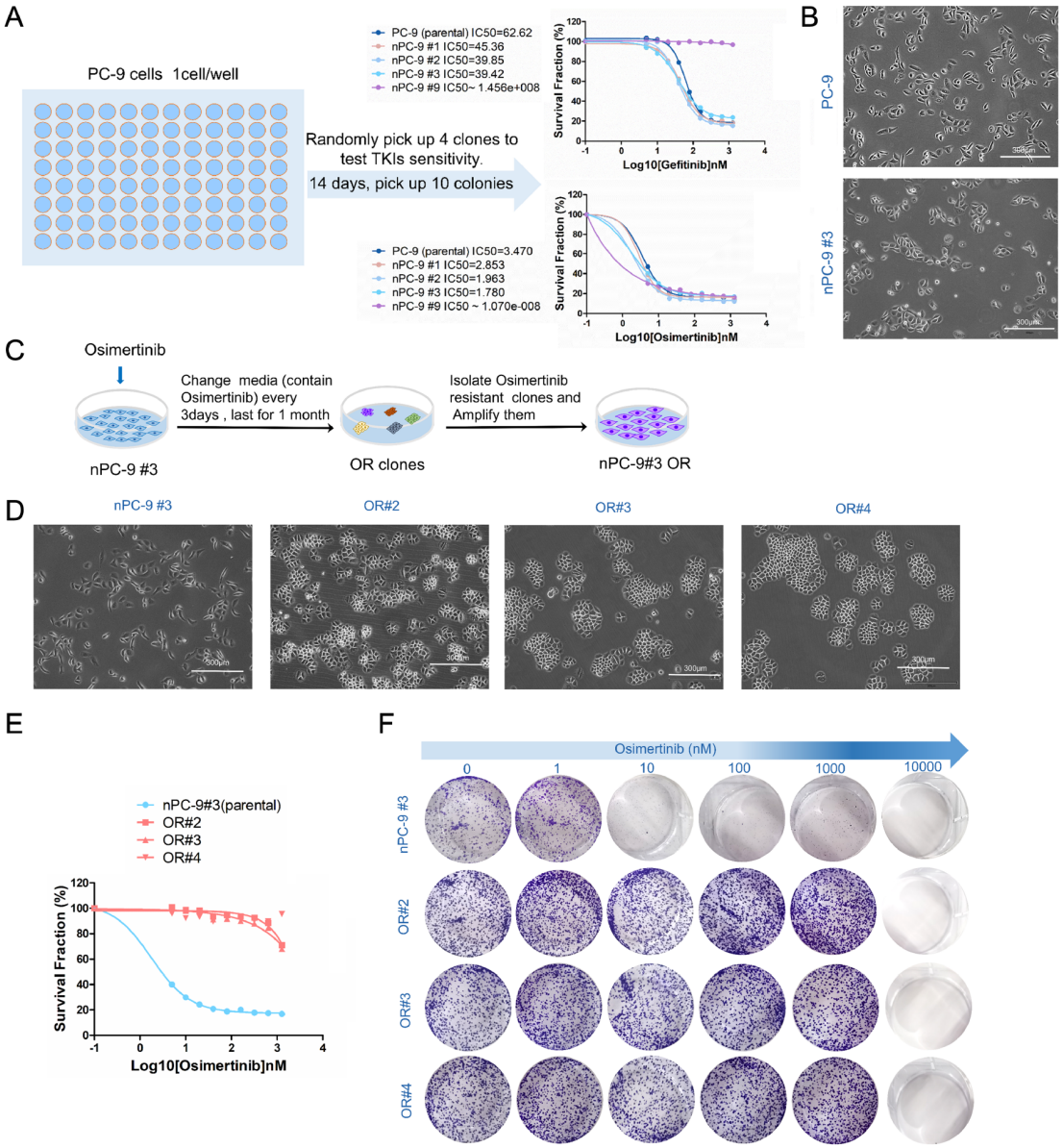


Figure 1. Establishment of naïve PC-9 single-cell clones and OR cell clones (A) Schematic representation of the establishment of single-cell clones and their sensitivity to EGFR-TKIs. PC-9 cells were seeded into 96-well plates (1 cell/well) and expanded, and individual clones were isolated. Four single-cell clones (naïve PC-9, nPC-9) were randomly selected and treated with gefitinib and osimertinib for 72 h. Cell viability was measured using the CCK-8 assay, and IC_{50} values were calculated using GraphPad Prism 5.0. (B) Morphological characteristics of nPC-9#3 and parental PC-9 cells. Scale bar: 300 μm. (C) Establishment of OR cells. nPC-9#3 cells were treated with a lethal concentration of osimertinib for one month, after which resistant clones were isolated and expanded. (D) Morphological features of OR cells. Scale bar: 300 μm. (E,F) Resistance of OR cells to osimertinib. nPC-9#3 parental cells and three OR clones were seeded into 96-well plates (3000 cells/well) and treated with varying concentrations of osimertinib for 72 h. Cell viability was measured using a CCK-8 assay after 72 h of treatment. In the colony formation assay, cells were seeded into 6-well plates (200 cells/well) and treated with the indicated concentrations of osimertinib. After 14 days, colonies were fixed and stained with crystal violet.

enhances their drug sensitivity. To further investigate this possibility, we assessed the effects of the HDAC6-specific inhibitor TAA in combination with osimertinib in OR cells. Our OR cell line displayed a nearly 100-fold resistance index compared to PC-9 wild-type (WT) cells (Figures 1F and 4A). Additionally, WT cells were more sensitive to TAA than OR cells (Figure 4B), likely due to higher HDAC6 expression in the OR cells.

Treatment with varying concentrations of TAA and osimertinib for 72 h showed that the combination of 5000 nM osimertinib with 3.125 μM, 6.25 μM, and 12.5 μM TAA significantly increased osimertinib sensitivity in OR cells ($P < 0.05$; Supplementary Figure S7). Using SynergyFinder (version 3.0), we calculated an SL score of 6.981 in OR cells, indicating an additive effect between TAA and osimertinib (Figure 4C). The additive effect of the two drugs was further confirmed by the colony formation assay. The combination of osimertinib and TAA demonstrated a stronger cytotoxic effect on OR cells than either drug used alone (Figure 4D,E). In summary, the use of an HDAC6 inhibitor in conjunction with osimertinib

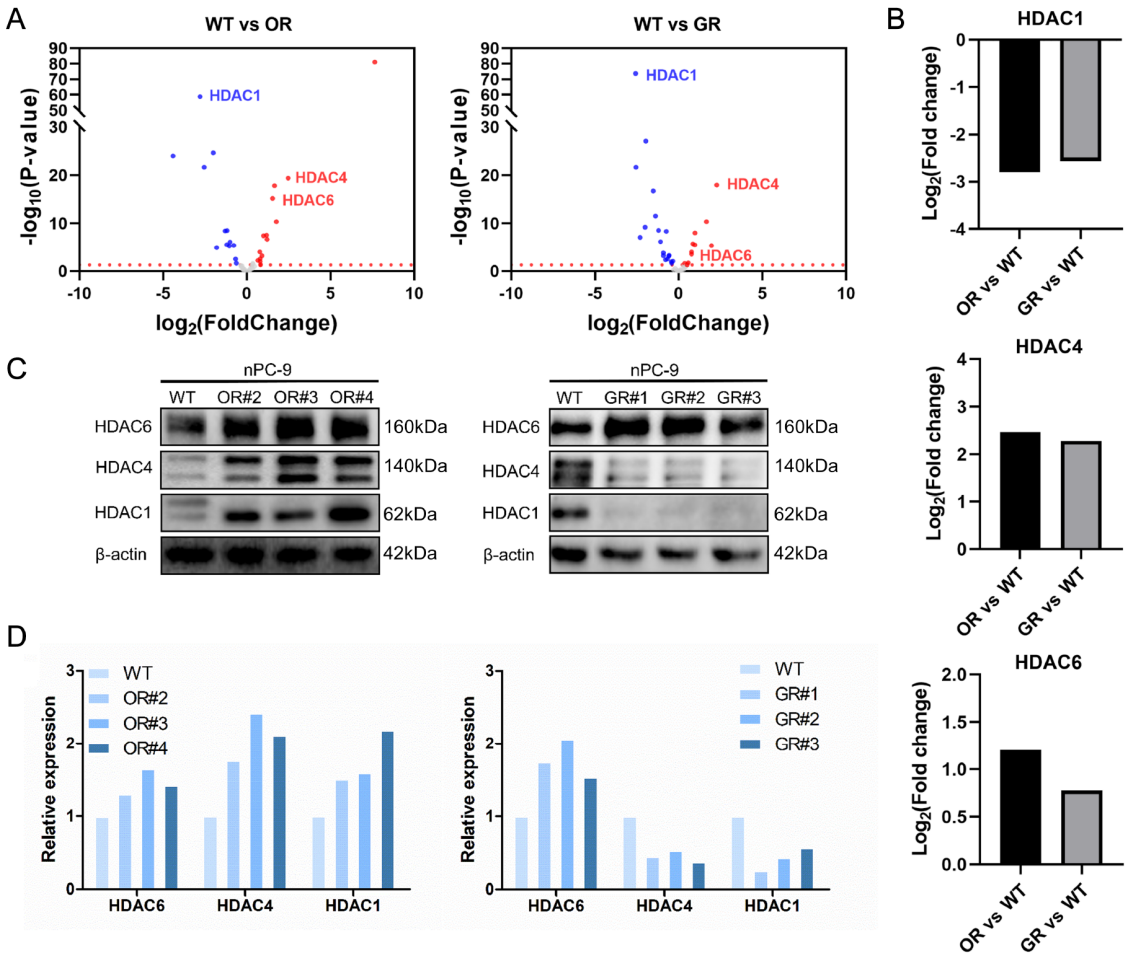


Figure 2. HDAC6 is upregulated in OR cells at the transcriptional and protein levels (A) Volcano plot of differentially expressed genes (DEGs) related to epigenetics. RNA-Seq was performed on the PC-9 WT, OR and GR groups. Genes associated with epigenetic regulation are highlighted in the volcano plot, using |log2FC| = 0.5849 (FC = 1.5) and $P = 0.05$ as the cutoff criteria. Genes with log2FC > 0.5849 and $P < 0.05$ were defined as upregulated, while those with log2FC < –0.5849 and $P < 0.05$ were defined as downregulated. Red dots represent significantly upregulated genes, while blue dots indicate significantly downregulated genes. In both the OR and GR groups, HDAC4 and HDAC6 were upregulated, whereas HDAC1 was downregulated. (B) Transcriptional fold change of HDAC1, HDAC4 and HDAC6. Bar plot shows the log2FC of HDAC1, HDAC4 and HDAC6 in OR/WT and GR/WT comparisons. (C) Western blot analysis of HDAC1, HDAC4 and HDAC6 protein levels. Protein expression of HDAC1, HDAC4 and HDAC6 was examined in WT, OR clones and GR clones. HDAC6 protein was consistently upregulated in both the OR and GR groups. (D) Relative protein expression levels of HDAC1, HDAC4 and HDAC6 in parental PC-9 (WT) cells, OR clones and GR clones, as quantified from immunoblot analysis. Values are normalized to WT (set as 1.0).

enhances the sensitivity of OR cells to osimertinib.

HDAC6 inhibitor delays PC-9 osimertinib resistance evolution

Our findings demonstrate that HDAC6 inhibition not only restores osimertinib sensitivity in resistant cells but also reveals time-dependent HDAC6 upregulation specifically in osimertinib-treated NSCLC cells, with no significant changes observed in pulmonary epithelial cells (Figure 5A and Supplementary Figure S8).

Building on this, we examined the effects of combining osimertinib with TAA. Using SynergyFinder, we calculated a synergy score (SL score) of 17.842, indicating significant synergistic effects between the two agents (Figure 5B). Clonogenic assay confirmed this synergistic effects (Figure 5C,D). Flow cytometric analysis showed that the combination of TAA and osimertinib significantly increased apoptosis rate; specifically, the combination group exhibited 42.95% apoptosis compared to 22.91% in the osimertinib-only group (Figure 5E). Based on our findings, we further investigated the role of HDAC6 inhibition in the osimertinib resistance evolution model. In the OR evolution model (Figure 5F), the combination therapy not only significantly suppressed the size of resistant clones but also markedly reduced the total number of resistant colonies formed (Figure 5G–I).

Collectively, these data demonstrated that HDAC6 expression is upregulated during the early phase of osimertinib treatment. The initial coadministration of TAA potentiates apoptosis, thereby enhancing tumor cell elimination and mitigating the development of resistant clones.

Overexpression of HDAC6 decreases osimertinib sensitivity by downregulating EGFR expression levels

To elucidate the specific role of HDAC6 in osimertinib resistance, we established a PC-9 cell line with stable HDAC6 overexpression

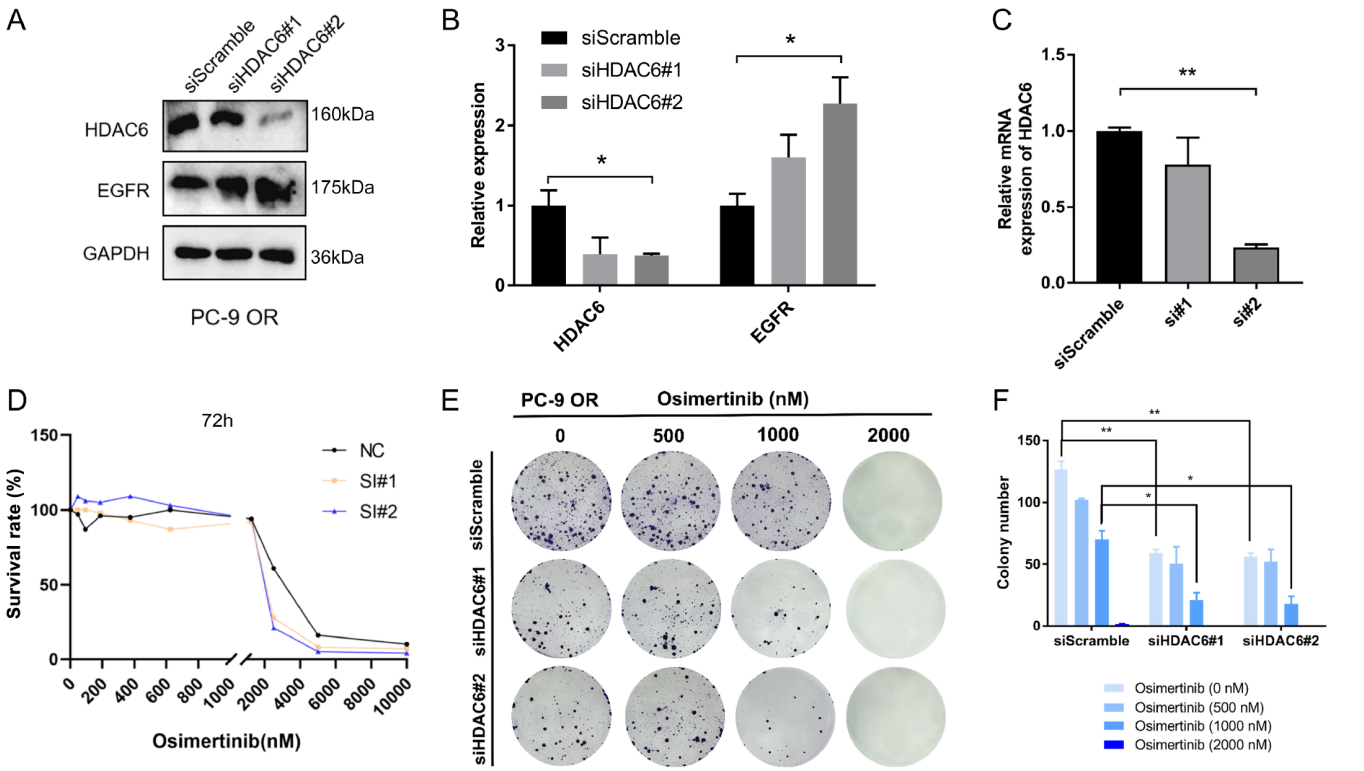


Figure 3. Knockdown of *HDAC6* by siRNA improves osimertinib sensitivity in OR cells (A) siRNA-mediated knockdown of *HDAC6* in OR cells was validated by western blot analysis. (B) Relative protein expression of HDAC6 and EGFR, normalized to β-actin. Band intensities were quantified using ImageJ, and data are presented as the mean ± SSD ($n = 3$). (C) siRNA-mediated knockdown of *HDAC6* in OR cells validated by RT-PCR. (D) Knockdown of *HDAC6* improves osimertinib sensitivity of OR cells. PC-9 OR cells were transfected with Scramble siRNA, siHDAC6#1 and siHDAC6#2. After 24 h of transfection, the cells were reseeded into 96-well plates (3000 cells/well). Cells were treated with varying concentrations of osimertinib for 72 h. Cell viability was measured using a CCK-8 assay. Cell survival fraction (SF; %) was calculated as follows: SF (%) = ($OD_{sample\ group}$ – $OD_{background}$) / ($OD_{control\ group}$ – $OD_{background}$) × 100%. (E) Knockdown of *HDAC6* improved osimertinib sensitivity. Cells were treated with siRNA after 48 h of transfection. Cells were reseeded (200 cells/well) in 6-well plates. After cells attached, cells were treated with varying concentrations of osimertinib (0, 500, 1000, and 2000 nM). After 14 days, colonies were fixed with methanol and stained with crystal violet. (F) Quantification of the colony formation assay. Crystal violet-stained colonies were solubilized with 10% acetic acid, and absorbance was measured at 570 nm using a microplate reader. The colony formation rate (%) was calculated as follows: Colony formation rate (%) = ($OD570_{Experimental\ group}$ – $OD570_{Blank}$) / ($OD570_{Control\ group}$ – $OD570_{Blank}$) × 100%. Data are presented as the mean ± SD. $n \geq 3$. Statistical significance was determined by one-way ANOVA. *$P < 0.05$, **$P < 0.01$.

(Figure 6A,B). In these HDAC6-overexpressing PC-9 cells, we observed that while HDAC6 overexpression did not significantly alter cell proliferation rates (Figure 6C and Supplementary Figure S9), it markedly enhanced the resistance of cells to osimertinib (Figure 6C–F). Notably, in PC-9 OR cells, elevated HDAC6 expression was accompanied by reduced EGFR levels (Supplementary Figure S10). Subsequent examination of EGFR expression in HDAC6-overexpressing cells revealed that HDAC6 overexpression similarly led to decreased EGFR protein expression (Figure 6G) without affecting *EGFR* mRNA level (Figure 6H). In conclusion, HDAC6 overexpression in osimertinib-sensitive cells induces both EGFR protein downregulation and osimertinib resistance. This mechanism likely underlines the acquired resistance observed in both OR cells and HDAC6-overexpressing cell lines.

HDAC6 regulates EGFR protein stability through the ubiquitin-proteasome pathway

HDAC6 overexpression significantly decreased EGFR protein abundance without altering its transcriptional level (Figure 6G,H), indicating posttranslational regulation. We thus hypothesized that HDAC6 facilitates EGFR degradation. To elucidate the underlying mechanism, we first determined whether HDAC6 physically interacts with EGFR. Co-IP analysis revealed no direct binding between HDAC6 and EGFR in either PC-9 HDAC6 OE cells (Figure 7A,B) or PC-9 OR cells (Supplementary Figure S11). We subsequently investigated whether HDAC6 promotes EGFR degradation through cycloheximide (CHX, 100 μg/mL)-mediated protein synthesis inhibition. To delineate the degradation pathway, cells were treated with either MG132 (a proteasome inhibitor) or chloroquine (CQ, a lysosome inhibitor). We found that CHX treatment led to time-dependent decrease of EGFR protein (Supplementary Figure S12). In HDAC6-OE cells, EGFR degradation was rescued by MG132 but not CQ, suggesting proteasomal dependency (Figure 7B,C). HDAC6 overexpression markedly attenuated EGFR degradation kinetics in the presence of CHX and MG132 (Figure 7B,C). Given that MG132 inhibits ubiquitin-proteasomal degradation, we further assessed EGFR ubiquitination. Notably, HDAC6-OE cells displayed substantially elevated EGFR polyubiquitination following 6 h of MG132 treatment (Figure 7D,E). These data demonstrate that HDAC6 does not engage in direct physical interaction with EGFR but governs its stability by augmenting ubiquitin–proteasome-mediated degradation.

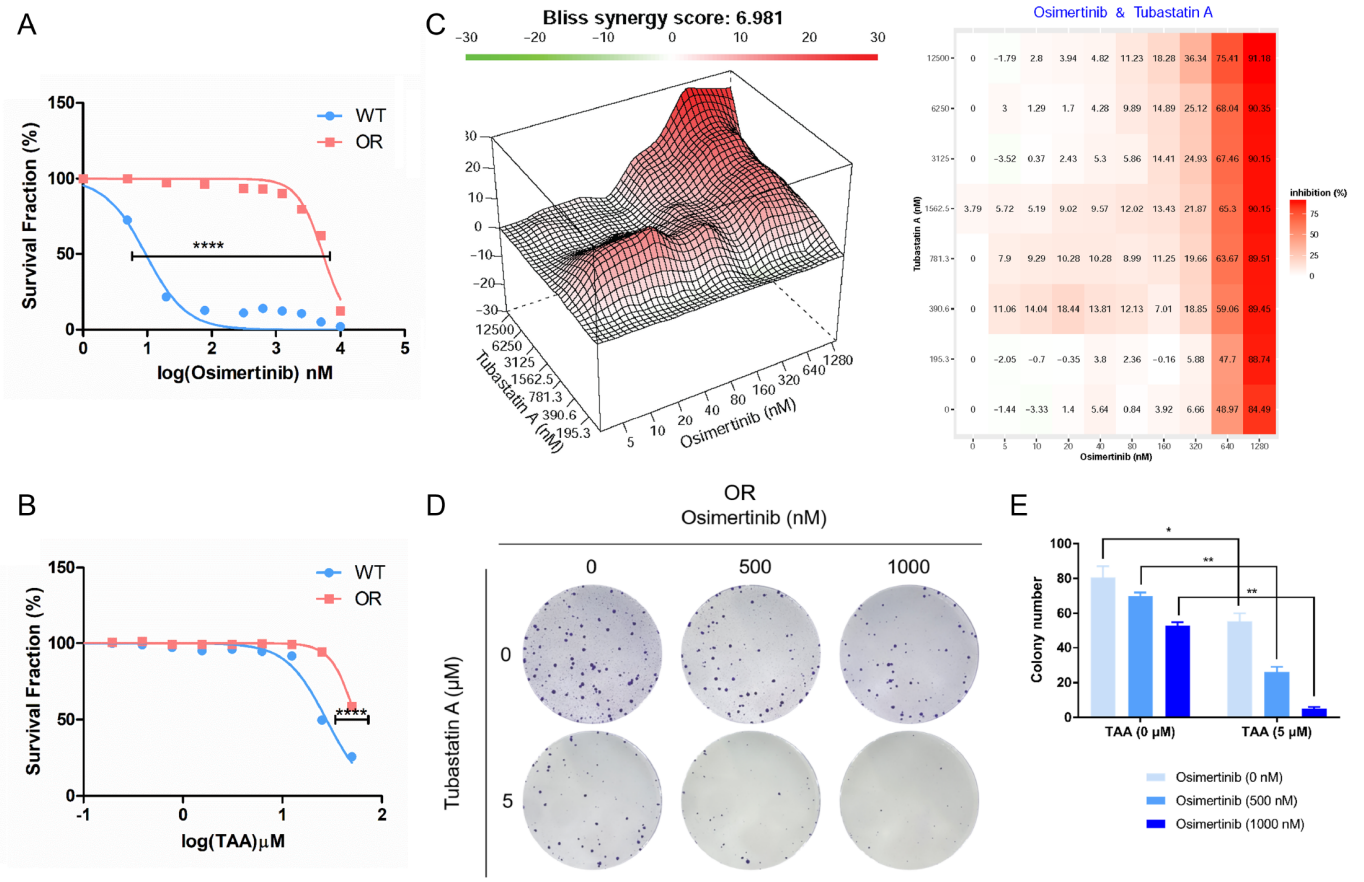


Figure 4. TAA enhances osimertinib sensitivity in OR cells (A,B) Dose-response curves of osimertinib and TAA sensitivity. PC-9 WT and OR cells were treated with the indicated concentrations of osimertinib or TAA for 72 h. Cell viability was assessed by CCK-8 assay. Data are presented as the mean ± SD of 3 independent experiments. Curves were fitted using a four-parameter logistic model. For osimertinib, the LogIC$_{50}$ value for OR cells was significantly higher than that for WT cells (extra sum-of-squares F test, ****$P < 0.0001$), and the calculated IC$_{50}$ values were 9.35 nM for WT and 5332 nM for OR cells. For TAA, the LogIC$_{50}$ value for WT cells was significantly higher than that for OR cells (extra sum-of-squares F test, ****$P < 0.0001$), and the calculated IC$_{50}$ values were 27.7 μM for WT and 55.21 μM for OR cells. (C) Additive effect of TAA and osimertinib in OR cells. Bliss synergy model analysis of osimertinib and TAA combination treatment in PC-9 OR cells. A positive Bliss score (6.981) indicates an additive effect. (D) Additive effect of osimertinib and TAA combination in PC-9 OR cells assessed by colony formation assay. Cells (200 cells/well) were seeded in 6-well plates and treated with varying concentrations of osimertinib and TAA. After 14 days, colonies were fixed with methanol and stained with crystal violet. (E) Quantification of the colony formation assay. Colony number was analyzed using ImageJ software, and the results are presented as colony number. Statistical significance was evaluated by Student's *t* test (for pairwise comparisons) or one-way ANOVA (for multigroup comparisons). *$P < 0.05$, **$P < 0.01$.

TAA combined with osimertinib effectively inhibits lung cancer organoid proliferation

Based on our findings that HDAC6 overexpression regulates EGFR protein levels and modulates osimertinib sensitivity in lung cancer cell lines, we further validated the combined therapeutic effect of HDAC6 inhibition and osimertinib using patient-derived lung cancer organoids. Our results demonstrate enhanced tumoricidal efficacy with this combinational approach. Using patient-derived lung cancer organoids (PDLOs), we treated them with osimertinib, TAA or osimertinib plus TAA, alongside a vehicle control (Figure 8A). Organoid growth was monitored throughout the treatment, with morphological changes documented by imaging. After 3 days of treatment, viability assay revealed that the TAA and control groups maintained robust growth, forming structurally intact organoids in Matrigel. In contrast, the osimertinib and osimertinib plus TAA groups exhibited markedly reduced growth rates and smaller organoid sizes (Figure 8B,C). The combination group showed further suppression compared to single-agent treatment, with significantly lower viability (Figure 8B,C). Further analysis revealed that the combination treatment significantly enhanced the apoptosis rate of lung cancer organoid cells (63.5% in the dual-drug combination group), whereas TAA monotherapy did not exert a significant impact on cell proliferation (Figure 8D,E). We also assessed the expression levels of HDAC6 and EGFR in drug-treated PDLOs. The results indicated that osimertinib treatment elevated HDAC6 protein expression, and combination therapy did not alter the total expression level of HDAC6 (Figure 8F). Collectively, HDAC6 inhibition synergizes with osimertinib to suppress PDLOs proliferation and partially overcome drug resistance.

Based on these findings, we propose the following working model (Figure 8G): during the development of osimertinib-acquired resistance, HDAC6 expression is upregulated, which promotes EGFR ubiquitination and degradation, leading to reduced or lost EGFR expression and thereby fostering the emergence of an EGFR loss-resistant subpopulation. Our study suggests that early-stage coadministration of an HDAC6 inhibitor

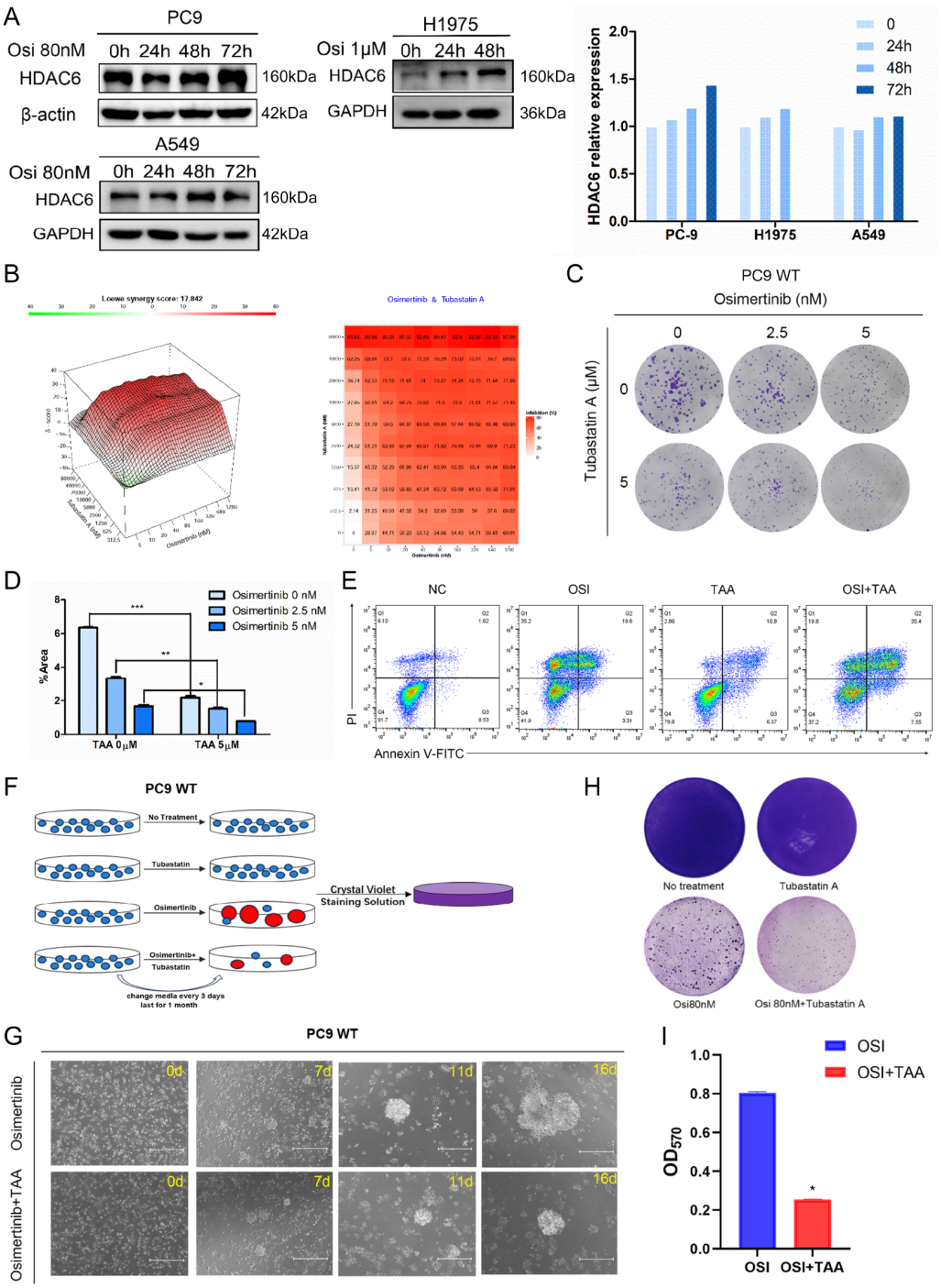


Figure 5. TAA delays/overcomes osimertinib resistance evolution in NSCLC cells (A) HDAC6 protein expression level upon osimertinib treatment in NSCLC. PC-9, H1975 and A549 cells were treated with the indicated concentrations of osimertinib for 24, 48, and 72 h. HDAC6 levels were measured by western blot analysis. Data are presented as the mean ± SD. (B) Synergistic effect of TAA and osimertinib in PC-9 cells. PC-9 cells were treated with varying concentrations of osimertinib ± TAA for 72 h. Cell viability was assessed by CCK8 assay, and synergy was quantified using SynergyFinder (Version 3.0, Loewe model). A Synergy Score (SL) > 10 indicates significant synergy. (C) Synergy effect of osimertinib and TAA combination in PC-9 cells was assessed by colony formation assay. Cells (200 cells/well) were seeded in 6-well plates and treated with varying concentrations of osimertinib and TAA. After 14 days, colonies were fixed with methanol and stained with crystal violet. (D) Quantification of the colony formation assay. Colony area was analyzed using ImageJ software, and the results are presented as % area. Statistical significance was evaluated by Student's *t* test (for pairwise comparisons) or one-way ANOVA (for multigroup comparisons). $^{*}P < 0.05$, $^{**}P < 0.01$, $^{***}P < 0.001$. (E) Detection of cell apoptosis. PC-9 cells were treated with 80 nM osimertinib alone or in combination with 10 μM TAA for 72 h. Apoptotic cells were labeled using Annexin V-FITC/PI double staining and analyzed by flow cytometry. (F) Flowchart of the effect of two drugs in the osimertinib resistance evolution model. (G) Naïve PC-9 cells were treated with osimertinib (80 nM) ± TAA (10 μM) for 1 month. The morphology of OR clones was observed for one month. Scale bar: 600 μm. (H,I) Naïve PC-9 cells were treated with osimertinib (80 nM) ± TAA (10 μM) for 1 month. Staining of resistant clones and quantification of former colonies. Statistical significance was determined using unpaired *t* test. $^{*}P < 0.05$.

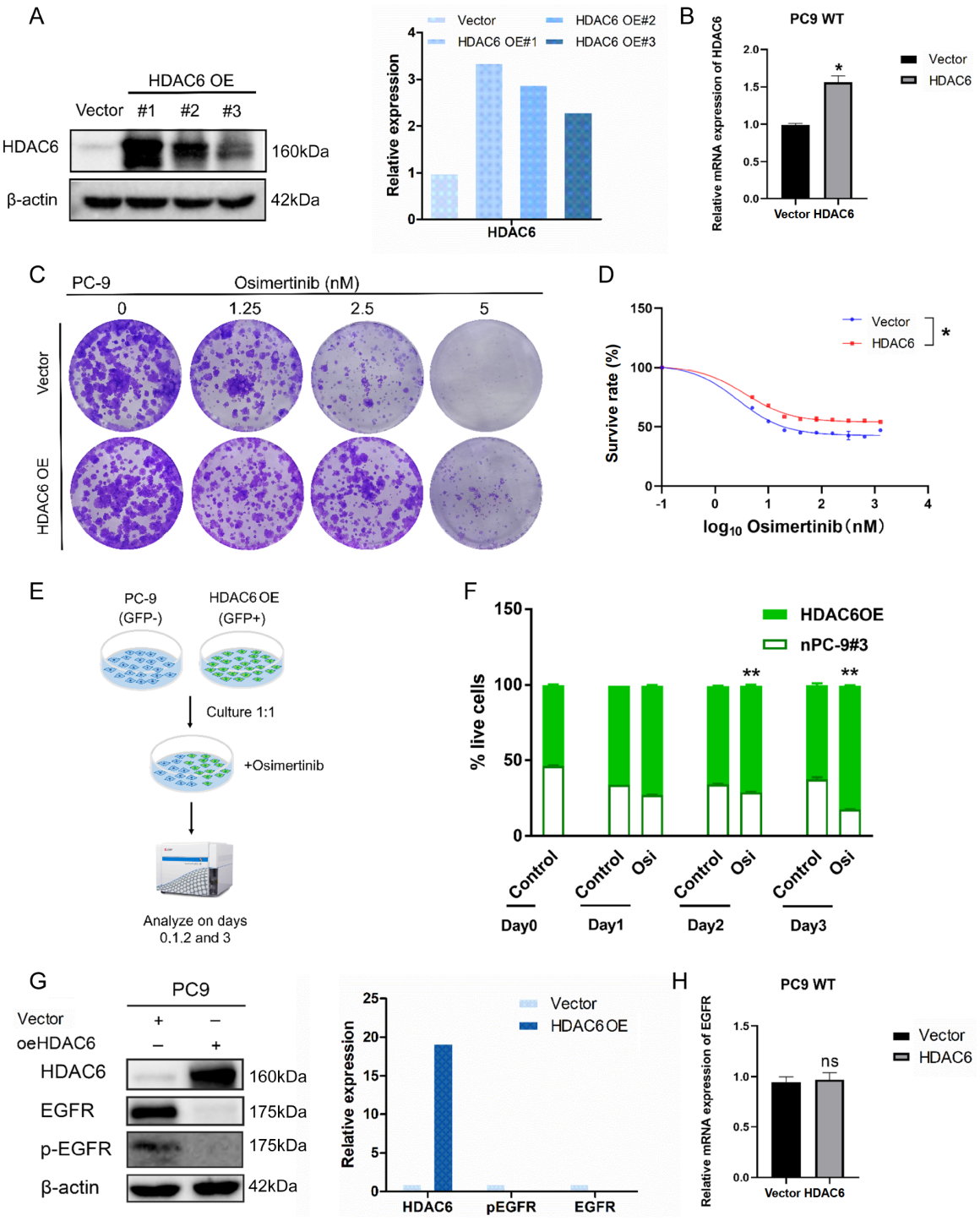


Figure 6. Overexpression of HDAC6 decreases osimertinib sensitivity by downregulating EGFR protein levels (A,B) Identification of HDAC6 overexpression in PC-9 cells. HDAC6 was overexpressed in PC-9 cells via transfection with plasmid pLV3-CMV-HDAC6 (human)-3×FLAG-CopGFP-Puro, followed by puromycin selection (1 μg/mL): HDAC6 protein levels were validated by western blot analysis in three randomly selected single-cell clones (A), and *HDAC6* mRNA levels were assessed by RT-PCR (B) in the bulk population 48 h post-transfection. Statistical significance was determined using Student's *t* test (for pairwise comparisons). $*P < 0.05$. (C,D) HDAC6 overexpression decreases osimertinib sensitivity. (C) Colony formation assay of cells stably overexpressing HDAC6 or empty vector (control) treated with the indicated concentrations of osimertinib. (D) Cell viability assessed by CCK-8 assay in HDAC6-overexpressing or vector control cells treated with osimertinib (96-well plates). Data are presented as the mean ± SD, and statistical significance was determined using Student's *t* test. $*P < 0.05$. (E,F) Osimertinib sensitivity assessed by competitive assay. (E) Schematic of the flow cytometry-based competition assay. (F) Quantification of live GFP-negative and GFP-positive cell percentages over time (days 0–3). Data are presented as the mean ± SD ($n = 3$ biological replicates). Statistical significance (unpaired *t* test) comparing GFP-positive cells to GFP-negative cells. $**P < 0.01$. (G,H) EGFR expression in HDAC6-overexpressing versus control cells. (G) Western blots showing reduced EGFR protein levels upon HDAC6 overexpression. (H) RT-PCR analysis confirming no significant change in mRNA levels. ns, not significant.

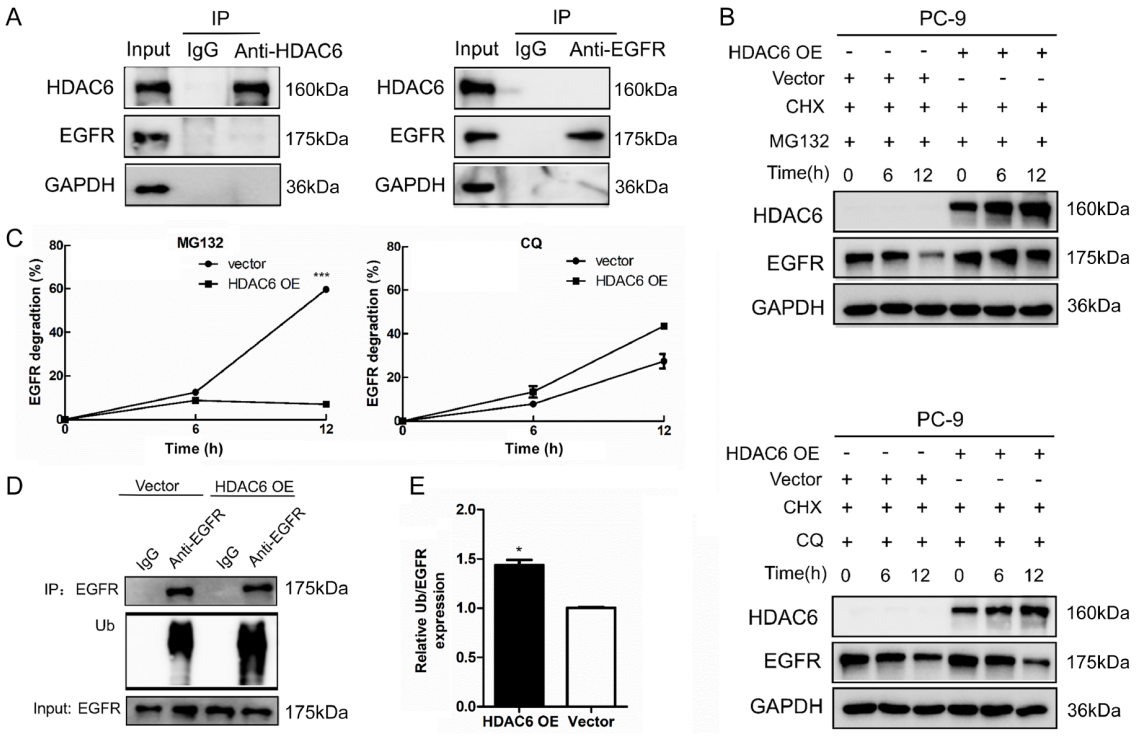


Figure 7. HDAC6 regulates EGFR degradation through the ubiquitin-proteasome pathway HDAC6 does not physically interact with EGFR. Co-IP assay was performed in PC-9 cells stably expressing HDAC6 or empty vector (control) following 6 h of treatment with MG132 (10 μM). Cell lysates were immunoprecipitated with anti-HDAC6 or anti-EGFR antibodies and immunoblotted for the indicated proteins. IgG served as a negative control. (B) HDAC6 promotes proteasome-dependent EGFR degradation. PC-9 cells overexpressing HDAC6 (HDAC6-OE) or empty vector were treated with cycloheximide (CHX, 10 μg/mL), MG132 (10 μM), or chloroquine (CQ, 50 μM) for the indicated durations (6 and 12 h). EGFR protein levels were assessed by western blot analysis. (C) Quantification analysis of EGFR degradation kinetics under proteasome or lysosome inhibition. Band intensities of EGFR and GAPDH (loading control) were quantified using ImageJ. Relative EGFR levels (normalized to GAPDH) at each time point are expressed as percentages of the 0-h baseline. Data are presented as the mean ± SD from two independent experiments. Statistical significance was determined by two-way ANOVA. ***$P < 0.001$. (D,E) HDAC6 enhances EGFR ubiquitination. (D) Cells were treated with MG132 (10 μM) for 6 h, followed by immunoprecipitation with anti-EGFR or control IgG antibodies and immunoblotting with anti-ubiquitin antibody. (E) Quantification of EGFR ubiquitination levels in HDAC6 OE versus vector control groups. Data are presented as the mean ± SD from two independent experiments. Statistical significance was determined by unpaired *t* test. *$P < 0.05$.

with osimertinib may effectively delay the formation of this resistant subtype, consequently prolonging the therapeutic efficacy of osimertinib.

In vivo antitumor efficacy of osimertinib combined with TAA

Following these *in vitro* studies, we next evaluated the antitumor efficacy of osimertinib combined with TAA *in vivo* using a PC9 xenograft model in BALB/c nude mice (Figure 9A). Tumor growth and body weight were measured throughout the treatment period. The combination of osimertinib and TAA significantly suppressed tumor growth compared to either monotherapy, which exhibited only limited effects (Figure 9B,C). Notably, TAA alone did not inhibit tumor progression, and the lack of a significant antitumor response to osimertinib as a single agent may be attributed to the relatively low dosage used in this study. Importantly, body weights of mice receiving the combination treatment remained comparable to those in other treatment groups (Figure 9D), indicating that the combination regimen was well tolerated.

We further assessed the effects of PC9/OR cells *in vivo*. PC9/OR cells successfully formed subcutaneous tumors in nude mice (Figure 9E,F). Importantly, these tumors maintained resistance to osimertinib treatment *in vivo* (Figure 9G), with no significant changes in body weight observed across groups (Figure 9H).

Discussion

The discovery of *EGFR* as a driver gene has facilitated the development of targeted therapeutic agents for lung cancer. Among these, the third-generation EGFR tyrosine kinase inhibitor (TKI) osimertinib has substantially improved clinical outcomes and quality of life in patients with advanced NSCLC [5]. However, the emergence of acquired resistance remains a major obstacle, severely limiting its long-term therapeutic efficacy [29]. To investigate the mechanisms underlying acquired resistance to osimertinib and to develop effective intervention strategies, we established an evolutionary cellular model of acquired drug resistance through *in vitro* drug pressure screening. Using this model, we obtained OR cell clones (Figure 1). In these resistant clones, loss of EGFR protein expression was identified as a key mediator of osimertinib resistance. Consistent with the loss of EGFR expression, the OR cells also exhibited strong cross-resistance to gefitinib (Supplementary Figure S13). Further mechanistic investigation revealed that elevated expression of histone deacetylase 6 (HDAC6) contributes to osimertinib resistance by regulating EGFR protein stability through the ubiquitin-proteasome pathway. Importantly, targeting HDAC6 was shown to delay the development of

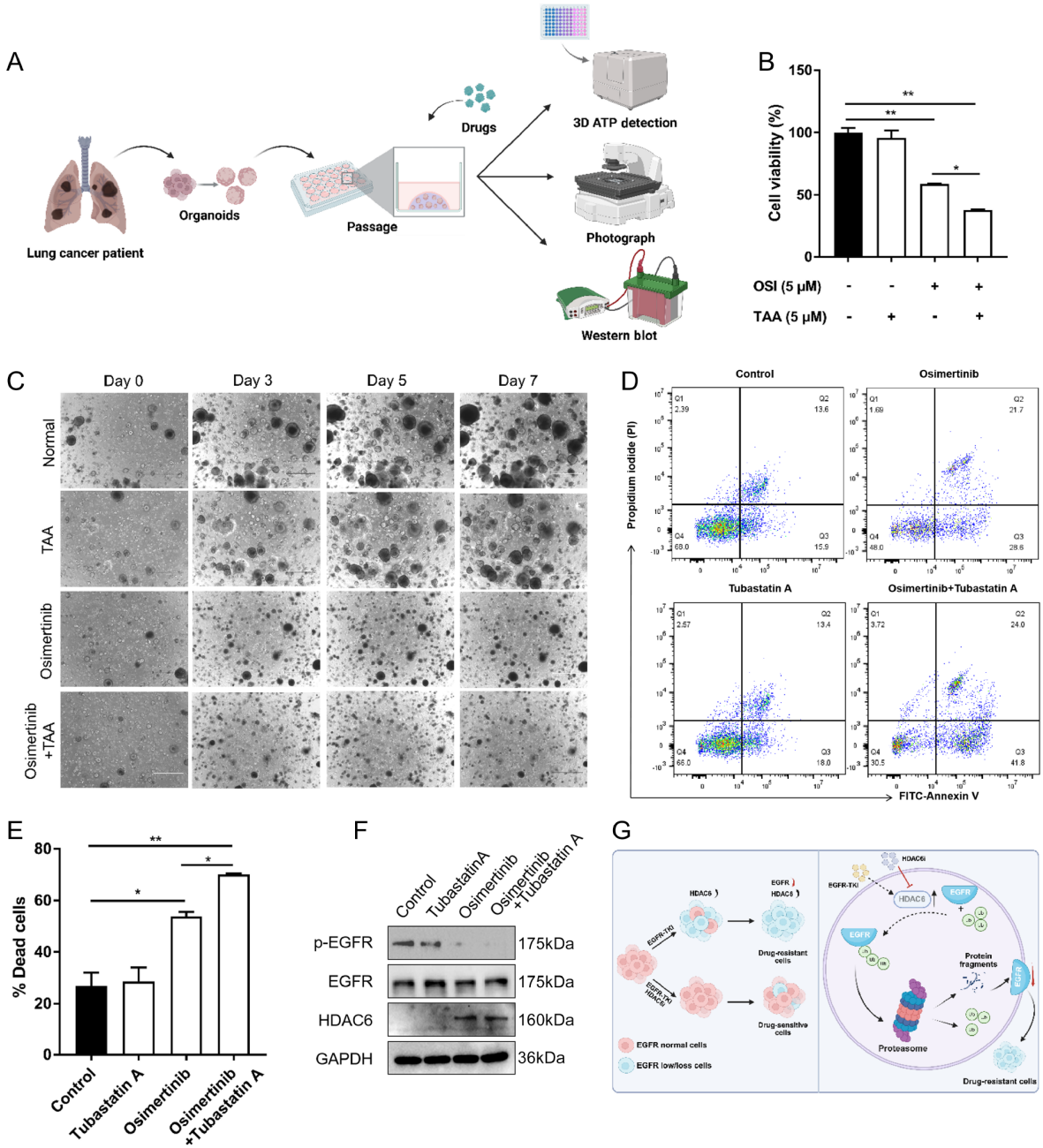


Figure 8. TAA increases osimertinib sensitivity in lung cancer organoids (A) Experimental workflow of lung cancer organoid study. Lung cancer organoids were established from a treatment-naïve patient with lung adenocarcinoma. The tumor tissue obtained via lung puncture harbors EGFR amplification and E746_A750 deletion. (B) Evaluation of TAA and osimertinib combination therapy in lung cancer organoids. Organoids were treated with osimertinib (5 μM) ± TAA (5 μM) for 72 h, followed by viability assessment. Data are presented as the mean ± SD from two independent experiments. Statistical significance was determined by one-way ANOVA. $*P < 0.05$, $**P < 0.01$. (C) Morphological changes of lung cancer organoids were observed at days 0, 3, 5, and 7 following treatment with osimertinib, TAA, or combination therapy. Scale bar: 750 μm. (D) Induction of apoptosis by combination therapy. Organoids treated for 3 days were analyzed for apoptosis using Annexin V-FITC/PI double staining followed by flow cytometry. (E) Quantification of total cell death by flow cytometry. $*P < 0.05$, $**P < 0.01$. (F) Expression levels of HDAC6 and EGFR in drug-treated lung cancer organoids. (G) Proposed working model of the study.

osimertinib resistance (Figure 5H). Of note, this effect was not limited to osimertinib, as HDAC6 inhibition similarly delayed the onset of gefitinib resistance (Supplementary Figure S14).

Acquired resistance to osimertinib is a complex process, with mechanisms broadly categorized into EGFR-dependent and EGFR-independent resistance [30,31]. EGFR-dependent resistance mechanisms include the emergence of resistance mutations (*e.g.*, C797S and other functional EGFR alterations) [7], EGFR gene amplification-mediated resistance [32,33], and loss of the primary drug-target mutation [34]. EGFR-independent resistance primarily involves the following two mechanisms [35,36]: bypass signaling activation, such as MET amplification (occurring in 5%–50% of

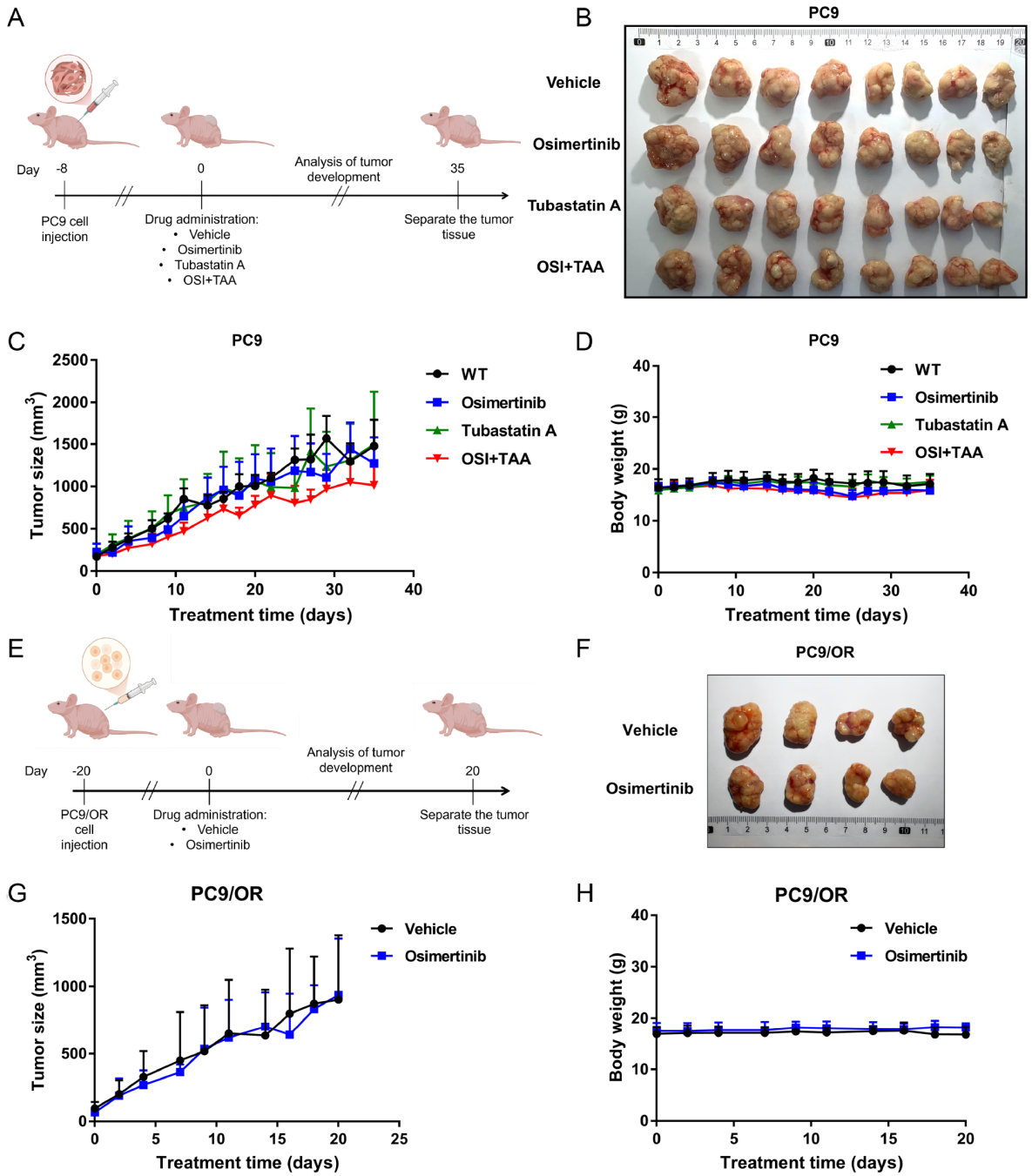


Figure 9. Effects of osimertinib and TAA on tumor growth in PC-9 xenograft model (A) Experimental timeline for PC-9 tumor-bearing mice. (B) Endpoint tumor volume of PC-9 model in vehicle, osimertinib, TAA and combination treated groups. n = 8. (C) Tumor volume curve in PC-9 xenografts treated with vehicle, osimertinib, TAA and combination therapy. Tumor size is shown in mm^3. (D) Body weight changes of PC-9 tumor-bearing mice during the treatment period, reflecting general tolerability of each treatment. (E) Experimental design of PC-9/OR tumor-bearing mice. Mice were treated with vehicle or osimertinib, followed by tumor development analysis and tissue collection. (F) Endpoint tumor volume of PC-9/OR xenografts in vehicle- and osimertinib-treated groups. n = 4. (G) Tumor growth curve of PC-9/OR xenografts treated with vehicle or osimertinib over time. Tumor size was measured at indicated time points. (H) Body weight changes of PC-9/OR tumor bearing mice during the treatment period, indicating drug safety and tolerability. Data are presented as the mean ± SD.

cases) and HER2 amplification (approximately 12%), which sustains tumor cell proliferation through alternative signaling pathways; and histologic transformation, including conversion to small cell lung cancer (SCLC) (3%–10%), accompanied by altered expression of neuroendocrine markers. In addition, enhanced cancer stem cell properties and epigenetic modifications (*e.g.*, RNA m5C/m6A methylation) mediate EGFR-independent resistance by regulating the expression of drug resistance-related genes. Collectively, these findings suggest that multitarget combination therapies or dynamic genetic monitoring may be required to

optimize postresistance treatment strategies.

The complexity and diversity of resistance mechanisms confer distinct "resistance subtypes" in clinically relapsed patients. Identifying and characterizing these subtypes is crucial for implementing precision medicine following resistance development in lung cancer patients. Previous studies have demonstrated intratumoral heterogeneity in EGFR protein expression, wherein cells with low EGFR expression exhibit greater tolerance to EGFR-TKIs than those with high EGFR expression, and this preexisting difference contributes to primary resistance [37]. However, whether an *EGFR*-deficient phenotype also exists in acquired resistance has remained unreported. In our study, using a high-dose "hard-hit" approach to generate resistant clones, we identified EGFR downregulation and loss as drivers of osimertinib resistance. We confirmed the presence of this resistant phenotype across multiple resistant clones (Figure 6 and Supplementary Figure S11). Nevertheless, clinical reports of EGFR protein loss-mediated acquired resistance in relapsed patients remain scarce. Although some studies have observed the disappearance of EGFR-sensitizing mutant proteins (*e.g.*, L858R or E746-A750del) in lavage fluid or lymph node biopsies from relapsed patients after targeted therapy, total EGFR protein levels were not significantly reduced [38]. Similarly, in AZD9291-treated relapsed patients, loss of the $EGFR^{LREAT747del/T790M}$ clone has been reported, but total EGFR protein levels were not assessed. We speculate that the lack of clinical reports on EGFR protein loss may stem from the following: (1) greater focus on newly acquired resistance mutations, which are more commonly detected and studied; and (2) limited availability of tissue biopsies post relapse, as liquid biopsies (*e.g.*, blood-based genotyping) are routinely used, leaving total EGFR protein levels unexamined. Based on our findings in resistant cell lines, we propose that EGFR target loss represents a distinct, albeit potentially rare, subtype of osimertinib-acquired resistance, warranting further validation and tailored therapeutic strategies. This conclusion requires confirmation in clinical patients.

To investigate the driving factors underlying EGFR downregulation under drug pressure, we performed RNA-Seq analysis on PC-9 WT and OR cells. This analysis revealed significant differences in the expression of epigenetic modification-related genes between the two cell types (Supplementary Figure S5). Given the established role of HDAC family members in lung cancer pathogenesis and treatment resistance [37], we further analyzed the expression profiles of HDAC family genes. Notably, HDAC6 transcript levels were significantly upregulated in OR cells and showed an inverse correlation with EGFR expression (Figure 2). To functionally validate the role of HDAC6, we employed RNAi-mediated *HDAC6* knockdown, which restored EGFR protein levels (Figure 3) and enhanced cellular sensitivity to osimertinib. Conversely, HDAC6 overexpression reduced EGFR protein levels and diminished drug sensitivity (Figure 6). Collectively, these findings demonstrate that HDAC6 promotes osimertinib resistance by negatively regulating EGFR protein stability. We further analyzed HDAC6 expression in lung adenocarcinoma (LUAD) using the TCGA database through the UALCAN platform. The results showed that *HDAC6* mRNA expression was significantly higher in LUAD tissue than in adjacent normal tissues ($P = 1.402 \times 10^{-6}$ Supplementary Figure S5). Further survival analysis indicated that LUAD patients with higher HDAC6 expression tended to have lower survival rates at later stages, although no significant impact on overall survival was observed ($P = 0.41$; Supplementary Figure S5). This finding aligns with our observation that in OR cells, HDAC6 primarily regulates EGFR expression at the level of protein stability, with minimal effect on its transcriptional activity. Therefore, we speculate that HDAC6 may play a partial role in osimertinib resistance and LUAD tumor progression, but its effect is not substantial enough to significantly affect patient overall survival.

In investigating the mechanism by which HDAC6 negatively regulates EGFR, we observed that short-term osimertinib treatment (24–72 h) induced a time-dependent upregulation of HDAC6 expression in non-small cell lung cancer cells (Figure 5). In OR cells, HDAC6 was significantly elevated at both the transcriptional and protein levels, whereas EGFR expression was downregulated (Supplementary Figure S11). In our established HDAC6-stably overexpressing cell lines, HDAC6 overexpression reduced EGFR protein levels (Figure 6F) without affecting its mRNA expression (Figure 6G), suggesting that HDAC6 primarily regulates EGFR protein stability rather than transcriptional activity. Notably, the observed transcriptional downregulation of EGFR in OR cells implies the existence of HDAC6-independent regulatory mechanisms. Therefore, the reduction in EGFR protein levels in OR cells is likely mediated by factors beyond HDAC6. This finding explains our observation that while the HDAC6 inhibitor TAA, when combined with osimertinib, reduced the formation of resistant clones in our resistance evolution model, it failed to completely abolish resistance development (Figure 5H,I). Based on these results, we conclude the following: (1) HDAC6 promotes resistance by modulating EGFR protein stability; (2) EGFR transcriptional downregulation is mediated by HDAC6-independent mechanisms; and (3) complete reversal of resistance would require simultaneous targeting of both HDAC6 and other unidentified factors.

HDAC6, a type IIB histone deacetylase, possesses two catalytic domains (CD1 and CD2) and a ubiquitin-binding zinc finger domain (ZnF-UBP), enabling it to mediate deacetylation and participate in the regulation of ubiquitinated protein degradation [39–41]. Our study revealed that although no direct binding was observed between HDAC6 and EGFR (Figure 7A and Supplementary Figure S12), HDAC6 overexpression promoted EGFR degradation by reducing protein levels via the ubiquitin-proteasome pathway (Figure 7B–E). This finding contrasts with previous reports indicating that HDAC6 stabilizes EGFR through α-tubulin acetylation [27,42], suggesting that HDAC6 may contribute to distinct resistant phenotypes under different mechanistic contexts. Thus, HDAC6 may exert bidirectional regulation on EGFR stability depending on the specific resistance mechanisms involved. We hypothesize that HDAC6 may modulate the activity of EGFR-specific E3 ligases through its deacetylation or ubiquitination functions, thereby enhancing ubiquitin-dependent EGFR degradation, a mechanism that warrants further validation in subsequent studies. Previous studies have shown that HDAC6 inhibition may serve as a broad-spectrum strategy to overcome drug resistance. The underlying mechanisms primarily include: (1) inducing autophagy through hyperacetylation of tubulin (*e.g.*, ACY-241) [43] and (2) stabilizing proapoptotic proteins such as Bim, as demonstrated in studies with the pan-HDAC inhibitor LBH589, which involved multiple resistance mechanisms, including MET amplification and T790M and C797S mutations [44]. The function of HDAC6 may extend beyond specific genomic backgrounds, with its central role in regulating the homeostasis of key proteins. Either by

influencing apoptotic proteins (*e.g.*, Bim) or the target protein itself (*e.g.*, EGFR), HDAC6 inhibition may restore cellular sensitivity to TKIs. Collectively, our work provides new insights for understanding the broad-spectrum anti-resistance effects of HDAC6 inhibitors.

Our study demonstrates that HDAC6 downregulates EGFR expression by promoting its ubiquitination and degradation, providing a theoretical basis for targeting HDAC6 to delay drug resistance. Currently, the development of HDAC6 inhibitors primarily focuses on its deacetylase and nonenzymatic functional domains, with several agents in clinical trials, including citarinostat (ACY-241) [43], ricolinostat (ACY-1215) [45], monohydrochloride (KA2507) [46], and purinostat mesylate (PM) [47]. These agents exhibit promising antitumor activity either as monotherapy or in combination regimens; however, no selective HDAC6 inhibitor has yet been approved for clinical use [36]. Notably, in our *in vitro* resistance evolution model, early coadministration of TAA and osimertinib significantly reduced the formation of resistant clones (Figure 5H,I). This synergistic effect was further validated in a lung cancer organoid model (Figure 8), suggesting that combining HDAC6 inhibitors with osimertinib may represent a potential strategy to overcome acquired resistance.

Our study demonstrates that high-dose "hard-hit" induction can generate resistant clones characterized by EGFR loss, in which HDAC6 plays a crucial role by promoting EGFR ubiquitination and subsequent degradation, ultimately leading to EGFR-deficient resistance. Importantly, targeting HDAC6 with osimertinib treatment shows the potential to delay resistance development (Figure 8F). Nevertheless, this study has certain limitations. First, the EGFR loss-resistant phenotype has not yet been clinically validated in real-world patient populations. Second, the precise molecular mechanism by which HDAC6 regulates EGFR ubiquitination requires further investigation.

Supplementary Data

Supplementary data are available at *Acta Biochimica et Biophysica Sinica* online.

Data Availability

The data that support the findings of this study are openly available in HARVARD Dataverse at https://doi.org/10.7910/DVN/4SBXNL. All other data can be accessed upon reasonable request from the corresponding author.

Acknowledgement

We thank Dr Xiangbo Jin from the Thoracic Surgery Research Center of The First Affiliated Hospital of Nanchang University for technical support with the xenograft experiments. We also thank Dr Yanan Wang and Dr Minzhang Cheng from the Jiangxi Provincial Center for Respiratory Diseases for helpful discussions and suggestions.

Author contributions

Xiaolei Li, Xinping Xu and Jun Che designed the research, wrote and reviewed the manuscript; Wei Zhang reviewed the manuscript; Cheng Yang, Danlei Xu, ZiFang Zhu, Kang Zhen and Kangkang Ren conducted experiments and analyzed the data; Yihan Yang Ye Huang conducted bioinformation analysis. All authors read and approved the final manuscript.

Funding

This work was supported by the grants from the China National Nature Science Foundation (Nos. 82560560, 31760038 and 32271324), and the National Science Foundation of Jiangxi Province (Nos. 20212BAB206034 and 20192BAB215032).

Conflict of Interest

The authors declare that they have no conflict of interest.

References

1. Bray F, Laversanne M, Sung H, Ferlay J, Siegel RL, Soerjomataram I, Jemal A. Global cancer statistics 2022: GLOBOCAN estimates of incidence and mortality worldwide for 36 cancers in 185 countries. *CA Cancer J Clin* 2024, 74: 229–263
2. Leiter A, Veluswamy RR, Wisnivesky JP. The global burden of lung cancer: current status and future trends. *Nat Rev Clin Oncol* 2023, 20: 624–639
3. Weinstein IB. Addiction to oncogenes—the achilles heal of cancer. *Science* 2002, 297: 63–64
4. Lynch TJ, Bell DW, Sordella R, Gurubhagavatula S, Okimoto RA, Brannigan BW, Harris PL, ***et al.*** Activating mutations in the epidermal growth factor receptor underlying responsiveness of non-small-cell lung cancer to gefitinib. *N Engl J Med* 2004, 350: 2129–2139
5. Cross DAE, Ashton SE, Ghiorghiu S, Eberlein C, Nebhan CA, Spitzler PJ, Orme JP, ***et al.*** AZD9291, an irreversible EGFR TKI, overcomes T790M-mediated resistance to EGFR inhibitors in lung cancer. *Cancer Discov* 2014, 4: 1046–1061
6. Mok TS, Wu YL, Ahn MJ, Garassino MC, Kim HR, Ramalingam SS, Shepherd FA, ***et al.*** Osimertinib or platinum-pemetrexed in *EGFR* T790M-positive lung cancer. *N Engl J Med* 2017, 376: 629–640
7. Ramalingam SS, Vansteenkiste J, Planchard D, Cho BC, Gray JE, Ohe Y, Zhou C, ***et al.*** Overall survival with osimertinib in untreated, *EGFR*-mutated advanced NSCLC. *N Engl J Med* 2020, 382: 41–50
8. Kim TM, Song A, Kim DW, Kim S, Ahn YO, Keam B, Jeon YK, ***et al.*** Mechanisms of acquired resistance to AZD9291. *J Thoracic Oncol* 2015, 10: 1736–1744
9. Oxnard GR, Arcila ME, Sima CS, Riely GJ, Chmielecki J, Kris MG, Pao W, ***et al.*** Acquired resistance to EGFR tyrosine kinase inhibitors in EGFR-mutant lung cancer: distinct natural history of patients with tumors harboring the T790M mutation. *Clin Cancer Res* 2011, 17: 1616–1622
10. Biedler JL, Riehm H. Cellular resistance to actinomycin D in Chinese hamster cells *in vitro*: cross-resistance, radioautographic, and cytogenetic studies. *Cancer Res* 1970, 30: 1174–1184
11. McDermott M, Eustace AJ, Busschots S, Breen L, Crown J, Clynes M, O′ Donovan N, ***et al.*** *In vitro* development of chemotherapy and targeted therapy drug-resistant cancer cell lines: a practical guide with case studies. *Front Oncol* 2014, 4: 40
12. Finn KJ, Martin SE, Settleman J. A single-step, high-dose selection scheme reveals distinct mechanisms of acquired resistance to oncogenic kinase inhibition in cancer cells. *Cancer Res* 2020, 80: 79–90
13. Schoenfeld AJ, Yu HA. The evolving landscape of resistance to osimertinib. *J Thoracic Oncol* 2020, 15: 18–21
14. Zhang L, Lu Q, Chang C. Epigenetics in health and disease. *Adv Exp Med Biol* 2020, 1253: 3–55
15. Shvedunova M, Akhtar A. Modulation of cellular processes by histone and non-histone protein acetylation. *Nat Rev Mol Cell Biol* 2022, 23: 329–349
16. Haberland M, Montgomery RL, Olson EN. The many roles of histone deacetylases in development and physiology: implications for disease and therapy. *Nat Rev Genet* 2009, 10: 32–42

17. Wang N, Ma T, Yu B. Targeting epigenetic regulators to overcome drug resistance in cancers. *Sig Transduct Target Ther* 2023, 8: 69
18. Banik D, Noonepalle S, Hadley M, Palmer E, Gracia-Hernandez M, Zevallos-Delgado C, Manhas N, *et al.* HDAC6 plays a noncanonical role in the regulation of antitumor immune responses, dissemination, and invasiveness of breast cancer. *Cancer Res* 2020, 80: 3649–3662
19. Ali A, Zhang F, Maguire A, Byrne T, Weiner-Gorzel K, Bridgett S, O'Toole S, *et al.* HDAC6 degradation inhibits the growth of high-grade serous ovarian cancer cells. *Cancers* 2020, 12: 3734
20. Liu B, Zhang J, Meng X, Xie SM, Liu F, Chen H, Yao D, *et al.* HDAC6-G3BP2 promotes lysosomal-TSC2 and suppresses mTORC1 under ETV4 targeting-induced low-lactate stress in non-small cell lung cancer. *Oncogene* 2023, 42: 1181–1195
21. Liang T, Wang F, Elhassan RM, Cheng Y, Tang X, Chen W, Fang H, *et al.* Targeting histone deacetylases for cancer therapy: trends and challenges. *Acta Pharm Sin B* 2023, 13: 2425–2463
22. Yu S, Cai X, Wu C, Liu Y, Zhang J, Gong X, Wang X, *et al.* Targeting HSP90-HDAC6 regulating network implicates precision treatment of breast cancer. *Int J Biol Sci* 2017, 13: 505–517
23. Wang L, Xiang S, Williams KA, Dong H, Bai W, Nicosia SV, Khochbin S, *et al.* Depletion of HDAC6 enhances cisplatin-induced DNA damage and apoptosis in non-small cell lung cancer cells. *PLoS One* 2012, 7: e44265
24. Yang WB, Hsu CC, Hsu TI, Liou JP, Chang KY, Chen PY, Liu JJ, *et al.* Increased activation of HDAC1/2/6 and Sp1 underlies therapeutic resistance and tumor growth in glioblastoma. *Neuro-Oncology* 2020, 22: 1439–1451
25. Hu C, Zhang M, Moses N, Hu C, Polin L, Chen W, Jang H, *et al.* The USP10-HDAC6 axis confers cisplatin resistance in non-small cell lung cancer lacking wild-type p53. *Cell Death Dis* 2020, 11: 328
26. Wang Z, Hu P, Tang F, Xie C. HDAC6-mediated EGFR stabilization and activation restrict cell response to sorafenib in non-small cell lung cancer cells. *Med Oncol* 2016, 33: 50
27. Wang Z, Tang F, Hu P, Wang Y, Gong J, Sun S, Xie C. HDAC6 promotes cell proliferation and confers resistance to gefitinib in lung adenocarcinoma. *Oncol Rep* 2016, 36: 589–597
28. Gu S, Liu Y, Zhu B, Ding K, Yao TP, Chen F, Zhan L, *et al.* Loss of α-tubulin acetylation is associated with TGF-β-induced epithelial-mesenchymal transition. *J Biol Chem* 2016, 291: 5396–5405
29. Zalaquett Z, Catherine Rita Hachem M, Kassis Y, Hachem S, Eid R, Raphael Kourie H, Planchard D. Acquired resistance mechanisms to osimertinib: the constant battle. *Cancer Treat Rev* 2023, 116: 102557
30. Leonetti A, Sharma S, Minari R, Perego P, Giovannetti E, Tiseo M. Resistance mechanisms to osimertinib in EGFR-mutated non-small cell lung cancer. *Br J Cancer* 2019, 121: 725–737
31. Zhu Z, Sun L, Li X, Xu X. Research progress on resistance mechanisms and therapeutic strategies against osimertinib in non-small cell lung cancer. *Cancer Research and Clinic* 2023, 35: 717-720
32. Ding X, Shi M, Liu D, Cao J, Zhang K, Zhang R, Zhang L, *et al.* Transformation to small cell lung cancer is irrespective of EGFR and accelerated by SMAD4-mediated ASCL1 transcription independently of RB1 in non-small cell lung cancer. *Cell Commun Signal* 2024, 22: 45
33. Dai HY, Chang LS, Yang SF, Wang SN, Su SJ, Yeh YT. HDAC6 promotes aggressive development of liver cancer by improving EGFR mRNA stability. *Neoplasia* 2023, 35: 100845
34. Oxnard GR, Hu Y, Mileham KF, Husain H, Costa DB, Tracy P, Feeney N, *et al.* Assessment of resistance mechanisms and clinical implications in patients with *EGFR* T790M-positive lung cancer and acquired resistance to osimertinib. *JAMA Oncol* 2018, 4: 1527–1534
35. Ciardiello F, Hirsch FR, Pirker R, Felip E, Valencia C, Smit EF. The role of anti-EGFR therapies in EGFR-TKI-resistant advanced non-small cell lung cancer. *Cancer Treat Rev* 2024, 122: 102664
36. Huang Z, Li L, Cheng B, Li D. Small molecules targeting HDAC6 for cancer treatment: current progress and novel strategies. *Biomed Pharmacother* 2024, 178: 117218
37. Alsaed B, Lin L, Son J, Li J, Smolander J, Lopez T, Eser PÖ, *et al.* Intratumor heterogeneity of EGFR expression mediates targeted therapy resistance and formation of drug tolerant microenvironment. *Nat Commun* 2025, 16: 28
38. Shellman YG, Tabara K, Kanda R, Sonoda K, Kubo T, Murakami Y, Kawahara A, Azuma K, *et al.* Loss of activating EGFR mutant gene contributes to acquired resistance to EGFR tyrosine kinase inhibitors in lung cancer cells. *PLoS One* 2012, 7: e41017
39. Seigneurin-Berny D, Verdel A, Curtet S, Lemercier C, Garin J, Rousseaux S, Khochbin S. Identification of components of the murine histone deacetylase 6 complex: link between acetylation and ubiquitination signaling pathways. *Mol Cell Biol* 2001, 21: 8035–8044
40. Zhu Y, Feng M, Wang B, Zheng Y, Jiang D, Zhao L, Mamun MAA, *et al.* New insights into the non-enzymatic function of HDAC6. *Biomed Pharmacother* 2023, 161: 114438
41. Zhang M, Xiang S, Joo HY, Wang L, Williams KA, Liu W, Hu C, *et al.* HDAC6 deacetylates and ubiquitinates MSH2 to maintain proper levels of MutSα. *Mol Cell* 2014, 55: 31–46
42. Deribe YL, Wild P, Chandrashaker A, Curak J, Schmidt MHH, Kalaidzidis Y, Milutinovic N, *et al.* Regulation of epidermal growth factor receptor trafficking by lysine deacetylase HDAC6. *Sci Signal* 2009, 2: ra84
43. Park SJ, Joo SH, Lee N, Jang WJ, Seo JH, Jeong CH. ACY-241, an HDAC6 inhibitor, overcomes erlotinib resistance in human pancreatic cancer cells by inducing autophagy. *Arch Pharm Res* 2021, 44: 1062–1075
44. Zang H, Qian G, Zong D, Fan S, Owonikoko TK, Ramalingam SS, Sun SY. Overcoming acquired resistance of epidermal growth factor receptor-mutant non-small cell lung cancer cells to osimertinib by combining osimertinib with the histone deacetylase inhibitor panobinostat (LBH589). *Cancer* 2020, 126: 2024–2033
45. Li J, Yu M, Fu S, Liu D, Tan Y. Role of selective histone deacetylase 6 inhibitor ACY-1215 in cancer and other human diseases. *Front Pharmacol* 2022, 13: 907981
46. Tsimberidou AM, Beer PA, Cartwright CA, Haymaker C, Vo HH, Kiany S, Cecil ARL, *et al.* Preclinical development and first-in-human study of KA2507, a selective and potent inhibitor of histone deacetylase 6, for patients with refractory solid tumors. *Clin Cancer Res* 2021, 27: 3584–3594
47. Zhu Z, Wen J, Xu Y, Pei H, Li D, Tang M, Bai P, *et al.* Therapeutic efficacy of an injectable formulation of purinostat mesylate in SU-DHL-6 tumour model. *Ann Med* 2022, 54: 743–753